İSTANBUL UNIVERSITY PRESS

Physics and Astronomy Reports
PAR 2024, 2 (2), 65–82
DOI: 10.26650/PAR.2024.00007

RESEARCH ARTICLE

An Updated Line List for Spectroscopic Investigation of G Stars - II: Refined Solar Abundances via Extended Wavelength Coverage to 10,000 Å

T. Şahin[1*,2], F. Güney[2], S.A. Şentürk[2], N. Çınar[2], and M. Marışmak[2]

[1] Akdeniz University, Faculty of Science, Department of Space Sciences and Technologies 07058, Antalya, Türkiye
[2] Institute of Graduate Studies in Science, Akdeniz University, Türkiye

ABSTRACT

This study introduces a line list for the abundance analysis of F-and G-type stars across the 4 080–9 675 Å wavelength range. A systematic search employing lower excitation potentials, accurate $\log gf$ values, and an updated multiplet table led to the identification of 592 lines across 33 species (25 elements), including C, O, Mg (ionized), Al, P, S, Cu, Zr (neutral), and La. To determine the uncertainties in $\log gf$ values, we assessed solar abundance using a very high-resolution (R ≈1 000 000) disk-integrated solar spectrum. These lines were confirmed to be blend-free in the solar spectrum. The line list was further validated by analyzing the metal-poor star HD 218209 (G6V), which is notable for its well-documented and reliable abundance in literature. The abundances were obtained using the equivalent width (EW) method and further refined by applying the spectrum synthesis method. A comparative analysis with the *Gaia*-ESO line list v.6, provided by the *Gaia*-ESO collaboration, revealed additional neutral and ionized Fe lines. This extensively refined line list will facilitate precise stellar parameter determinations and accurate abundance analyses of spectra within the PolarBASE spectral library.

Keywords: Line: identification; Sun: abundances; Sun: fundamental parameters; Stars: individual (HD 218209)

1. INTRODUCTION

Advancements in spectroscopic methodologies for G-type stars have enabled more precise elemental abundance measurements. High-resolution spectroscopic techniques enable researchers to analyze stellar spectra in detail, providing insights into their atmospheric compositions and the underlying nucleosynthesis processes (Sharma et al. 2018; Trevisan et al. 2021). Analysis of G-dwarfs revealed discrepancies between the observed and predicted abundance patterns, challenging existing galactic chemical evolution models (Woolf & West 2012). These findings highlights the importance of combining improved modelling techniques with high-resolution spectroscopic data.

G-type stars, including the Sun, serve as fundamental benchmarks for understanding the stellar evolution and galactic chemical history (Bensby et al. 2003; Heiter et al. 2015). Their relatively long lifetimes allow them to retain the chemical signatures of the molecular clouds from which they form (Bensby et al. 2003; Heiter et al. 2015; Aoki et al. 2022). Solar photospheric abundances, derived from spectroscopic observations, provide a reference point for abundance determination in metal-poor stars and are essential for understanding the processes that govern stellar and galactic evolution (Lodders 2003; Pagel & Patchett 1975). Recent studies have significantly advanced our understanding of solar abundance by incorporating various physical processes, such as gravitational settling, convective overshooting, solar wind mass loss, pre-main-sequence disk accretion, opacity, and helium abundance in the solar corona (Wang & Zhao 2013; Zhang et al. 2019; Karathanou et al. 2020; Asplund et al. 2021; Salmon et al. 2021).

Migration complicates the interpretation of their origins because it can result in metal-poor stars being found in regions where they are not typically expected (Haywood 2008). Zhang et al. (2019) explored the implications of convective overshoot, solar-wind mass loss, and pre-main-sequence disk accretion on solar models. Their findings indicate that incorporating additional physical processes significantly improves the alignment between solar models and helioseismic constraints, effectively addressing the solar abundance problem. Karathanou et al. (2020) demonstrated how updated abundances can influence the internal solar structure via critical solar quantities such as temperature and pressure.

Asplund et al. (2021) presented the updated solar photospheric and proto-solar abundances of 83 elements. Their work highlighted the so-called solar modelling problem, which refers to the persistent discrepancies between helioseismic observations and solar interior models constructed with low metallicity. This suggests that there may be shortcomings in the computed opacities or the treatment of mixing processes below the con-

Corresponding Author: Timur Şahin **E-mail:** timursahin@akdeniz.edu.tr
Submitted: 05.11.2024 • **Accepted:** 27.12.2024

vection zone in the existing models. The updated abundances are essential for refining our understanding of the solar structure and evolution, as they provide a more accurate baseline for the solar modelling problem.

Moreover, the variability in helium abundance in the solar corona, as discussed by Ofman et al. (2024), also plays a role in understanding solar atmospheric processes. This variability is crucial for interpreting solar observations and for understanding the dynamics of the solar atmosphere. This study presents a three-dimensional model that illustrates the influence of solar activity and coronal heating processes on helium abundance.

These updates are essential for addressing the solar modelling problem and refining our understanding of the solar structure and evolution. Addressing this complex problem requires precise atmospheric modeling supported by comprehensive and accurate line lists.

The author's research team has been actively studying G-type stars, particularly those in solar neighborhoods. In our previous work (Şahin et al. 2023, hereafter Paper I), we presented a line list covering the 4 080-6 780 Å wavelength range designed for the spectroscopic analysis of more than 90 G-type metal-poor stars residing within the solar neighborhood. Previous studies by the research team, such as Marışmak et al. (2024) and Şentürk et al. (2024), also utilized the line list presented in Paper I. For instance, Marışmak et al. (2024) employed this line list to analyze two metal-poor high-proper motion stars, HD 8724 and HD 195633, whereas Şentürk et al. (2024) used it for spectroscopic analysis of a solar analogue star in the optical region.

Building on this foundation, we now extend the wavelength coverage of the line list to 10 000 Å, enabling a more comprehensive spectroscopic analysis of G-type stars, particularly in the near-infrared region. Şentürk et al. (2024) presented a line list covering the 10 000-25 000 Å range, which will be valuable for future spectroscopic studies of G-type stars, including solar analogue and solar twin stars in the *H*- and *K*-bands.

The remainder of this paper is organized as follows. Section 2 provides the observational data. Section 3 explains the methodology, including line identification and measurement procedures, the determination of model parameters, and the techniques for chemical abundance analysis of both HD 218209 and the Sun. Section 4 presents the line list, including details on line identification, measurement, and the atomic data used in the analysis. Finally, Section 5 summarizes our findings and discusses their implications.

2. OBSERVATIONS

This study analyzes high-resolution spectra of the Sun and HD 218209 to develop and validate a line list. Compared with Paper I, this study significantly expands the scope of spectral analyses by extending the analysis to the near-infrared region. For HD 218209, a high-resolution ($R \approx 76\,000$) and high signal-to-noise ratio ($S/N = 156$) PolarBASE[1] (Petit et al. 2014) Narval[2] spectrum (HJD 2456232.48238; exposure time of 400 s) obtained from the PolarBASE archive. The characteristics of the HD 218209's spectrum and KPNO solar spectrum are displayed in Figure 1.

The spectrum was continuum-normalized and corrected for radial velocity ($V_{\rm Rad}$) before line measurements. The Python interface and synthetic Narval solar spectra, which include atomic transitions in the range of 3 700–10 048 Å were used for RV correction ($V_{\rm Rad}$ = 16.03 km s^{-1}), and the renormalization process was performed using the LIME code developed in the IDL environment (Şahin 2017). Lines with equivalent widths (EW) below 5 mÅ or above 200 mÅ were excluded from the analysis.

The solar spectrum serves as a fundamental reference for stellar astrophysics and analysis of physical processes in stars (Molaro & Monai 2012). In this study, high-resolution ($R \approx 700\,000$) Kitt Peak Fourier Transform Spectrometer (FTS) data (disk-integrated) obtained by Kurucz et al. (1984), previously utilized by Şahin et al. (2023), and a very high-resolution ($R \approx 1\,000\,000$) disk-integrated Göttingen (IAG)[3] solar flux atlas[4] obtained by Baker et al. (2020) with Vacuum Vertical Telescope (VVT) were used. However, it should be noted that an alternative link[5] was also provided by Baker et al. (2020). Differences[6] were observed between the two spectra (see Appendix for Figure A1). The KPNO solar spectrum was used for analyses in the 4 000-5 000 Å range, while the telluric-free IAG solar spectrum (BTFS) was preferred for the 5000-10000 Å range. Hence, both solar spectra have enabled line identification and other classical spectral analysis methods over the entire 4 000-10 000 Å wavelength range. Although the KPNO spectrum is reliable, it contains telluric lines within the ELODIE wavelength range; in particular, around 6 000 Å. In the longer wavelength regions, telluric bands caused by H_2O and molecular O_2 are prominent (see Figure 2 for details). In the KPNO solar spectrum, transitions outside the regions dominated by telluric lines were considered for the line list created in Paper I of the series, which covered 4 000-6 800 Å range. The 5 000-6 800 Å wavelength region is common between the KPNO and IAG (BTFS) solar spectra. We compared the equivalent widths (EW) of the lines in this region and found that the EW measurements of the two spectra were in good agreement [EW(KPNO) = (0.956±0.011)× EW(IAG)+(2.353±0.839)].

3. THE ABUNDANCE ANALYSIS

The elemental abundances were determined using the local thermodynamic equilibrium (LTE) line analysis code, MOOG

[1] http://polarbase.irap.omp.eu
[2] Narval spectropolarimeter is adapted to the 2m Bernard Lyot telescope and provides high-resolution spectral and polarimetric data.
[3] IAG: Institute for Astrophysics, Göttingen.
[4] BTFS; https://zenodo.org/records/3598136
[5] zenodo; https://web.sas.upenn.edu/ashbaker/solar-atlas/
[6] Ashley Baker; private communication

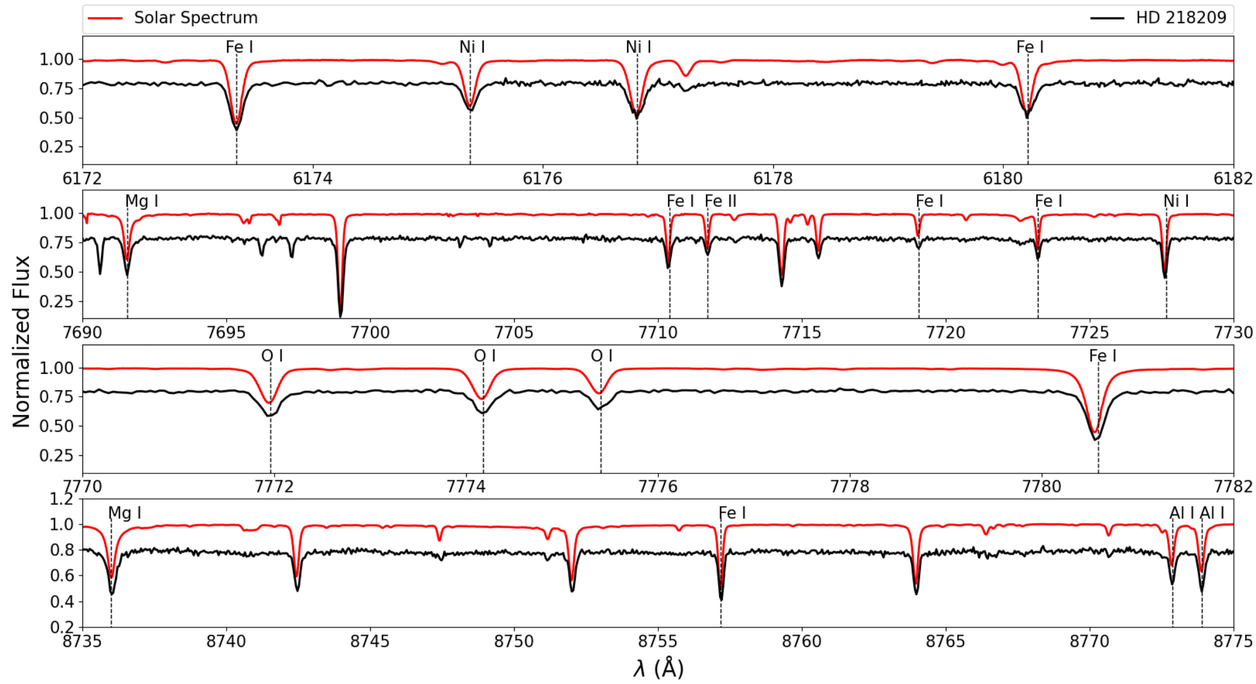

Figure 1. A small region of the KPNO solar spectrum and the PolarBASE spectrum of HD 218209. Identified lines are also indicated.

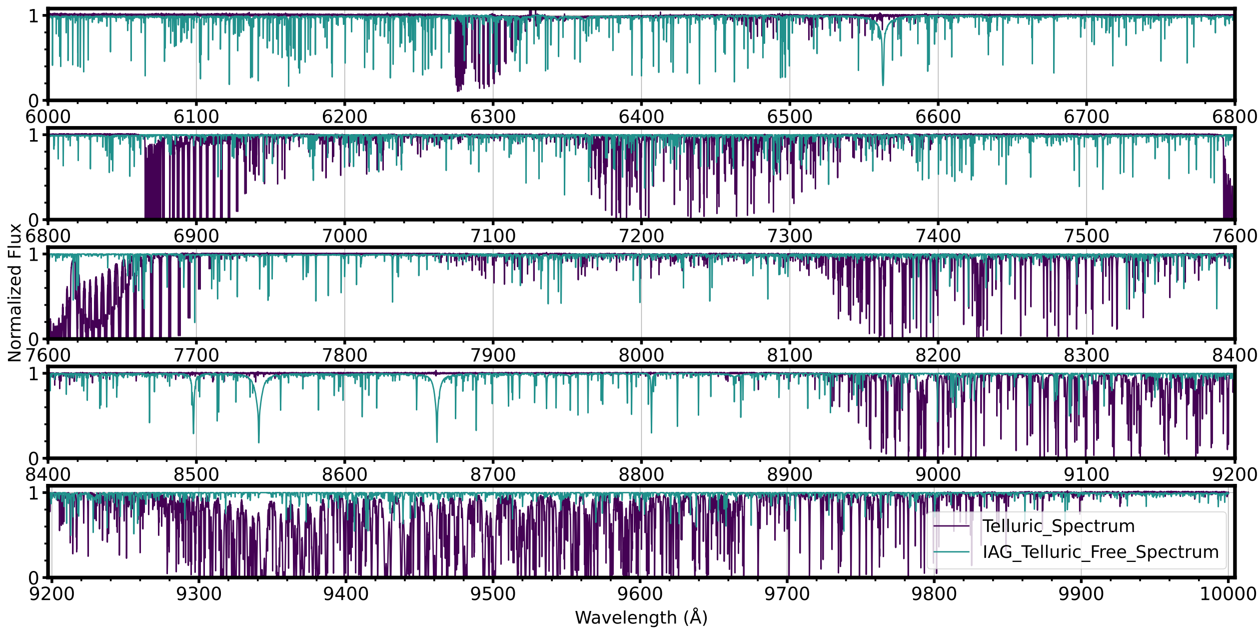

Figure 2. The telluric corrected Göttingen (IAG) Solar Spectrum (BTFS). Telluric spectrum (from `https://zenodo.org/records/3598136`) was also included to indicate the positions of the telluric lines. The telluric model shown is typical of the conditions at Göttingen (precipitable water vapour of ≈10 mm), where the VVT telescope resides.

(Sneden 1973)[7]. Model atmospheres were generated using ATLAS9 code (Castelli & Kurucz 2003) with the LTE (ODFNEW) approach. Detailed descriptions of the abundance analysis procedure have been provided by Şahin & Lambert (2009), Şahin et al. (2011), Şahin et al. (2016), Şahin & Bilir (2020), and Şahin et al. (2023). The atmospheric parameters of the model, such as the effective temperature ($T_{\rm eff}$), surface gravity (log g), metallicity ([Fe/H]), and microturbulent velocity (ξ), were determined using neutral (Fe I) and ionized (Fe II) iron lines in an iterative process. The $T_{\rm eff}$ determination employed the excitation balance method (sensitive to neutral spectral lines with a

[7] The source code for MOOG can be accessed at `http://www.as.utexas.edu/chris/moog.html`

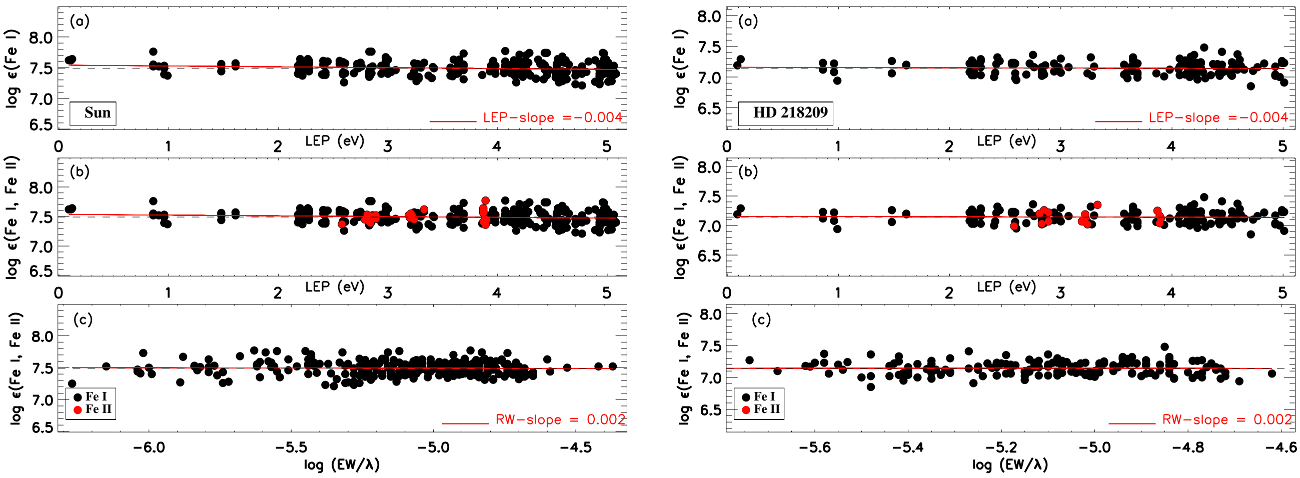

Figure 3. An example for the determination of the atmospheric parameters $T_{\rm eff}$ and ξ using abundance (log ϵ) as a function of both lower LEP (panels a and b) and reduced EW (panels c) for the Sun and HD 218209. In all panels, the solid red line represents the least-squares fit to the data.

broad range of excitation potentials) for Fe I. ξ represents the small-scale gas motion within the stellar atmosphere. ξ was determined by ensuring that the abundance of Fe atoms (Fe I) remained independent of the reduced equivalent width (EW/λ) under the assumption of LTE. These two conditions were simultaneously applied to a set of Fe I lines (see Figure 3, upper and middle panels). In addition, ξ is determined using a dispersion test for a given model atmosphere (Figure A2). This involved computing the dispersion in abundance (Fe, Ti, Cr) over the range of 0.0 to 3.0 km s^{-1}. By combining both methods, the measurement uncertainty for ξ was estimated as 0.5 km s^{-1} (Figure A2). In the same figure, an example Kiel diagram is included.

Surface gravity (log g) was determined by analyzing Fe abundances calculated with MOOG, ensuring ionization equilibrium where Fe I and Fe II lines yield the same abundance. Notably, in the solar spectrum, ionization equilibrium is achieved between the neutral and ionized atoms of Mg, Sc, Ti, Cr, and Zr. Similarly, in the spectrum of HD 218209, in addition to Fe, ionization equilibrium is reached for Ti and Cr. Finally, the metallicity ([Fe/H]) was refined through an iterative process to achieve convergence between the derived Fe abundance and the initial abundance adopted for the model atmosphere construction. Convergence was achieved by adjusting $T_{\rm eff}$, log g, and ξ of the model. Figure 3 illustrates a summary of the relationship between the physical parameters used to determine the stellar model parameters using the classical spectroscopic method (i.e., ionization and excitation equilibria of the Fe lines) for the Sun (left panel) and HD 218209 (right panel).

The uncertainty in the derived $T_{\rm eff}$ originates from the error associated with the slope of the relationship between the Fe I abundance and the LEPs of the lines. Additionally, a 1σ difference in abundance ([X/H]) between the Fe I and Fe II lines corresponds to a change in 0.19 dex in log g. Table 1 summarizes the resulting model parameters for HD 218209 and the Sun. The uncertainties in the atomic data (log gf values) were

Table 1. Model atmosphere parameters for HD 218209, and the Sun.

Star	$T_{\rm eff}$ (K)	log g (cgs)	[Fe/H] (dex)	ξ (km s^{-1})
HD 218209	5600^{+177}_{-177}	$4.50^{+0.24}_{-0.24}$	$-0.36^{+0.13}_{-0.13}$	$0.44^{+0.50}_{-0.50}$
Sun †	5770^{+130}_{-130}	$4.40^{+0.19}_{-0.19}$	$0.00^{+0.09}_{-0.09}$	$0.66^{+0.50}_{-0.50}$
Sun *	5790^{+45}_{-45}	$4.40^{+0.09}_{-0.09}$	$0.00^{+0.04}_{-0.04}$	$0.66^{+0.50}_{-0.50}$

(†): This study (TS), the solar spectrum was provided by Baker et al. (2020).
(*): The atmospheric parameters from Şahin et al. (2023). The solar spectrum was obtained from Kurucz et al. (1984).

assessed by deriving solar abundances from the stellar spectral lines. The solar model derived from our analysis yielded the following atmospheric parameters: $T_{\rm eff}$ = 5770 K, log g = 4.40 cgs, [Fe/H] = 0.00 dex, and ξ = 0.66 km s^{-1}. These values are in good agreement with the standard solar models. The abundances obtained for the solar photosphere as a result of solar analysis were calculated using these model parameters (Table 1). In Table 1, the solar abundances reported by Asplund et al. (2009, 2021) are also included. In Table 2, we provide a summary of element abundances based on the model parameters in LTE. log ϵ is the logarithm of abundance. The errors reported in log ϵ abundances are represented by 1σ line-to-line scatter in abundance. [X/H] is the logarithmic abundance ratio of hydrogen to the corresponding solar values and [X/Fe] is the logarithmic abundance considering the abundance of Fe I. The error in [X/Fe] is the square root of the sum of the quadratures of the errors in [X/H] and [Fe/H]. Table 2 presents the abundances obtained using PolarBase spectrum of the star as a function of the [X/Fe] ratio.

An analysis of the chemical abundances of 33 species belonging to 27 elements, as presented in Table 2, was consistent

Table 2. The abundances of the observed species for Sun and HD 218209. The solar abundances obtained in this study and those reported by Asplund et al. (2009, ASP09) and Asplund et al. (2021, ASP21) are also provided. Abundances in bold are those calculated via the spectrum synthesis method.

	HD 218209			Sun											
Species	$[X/Fe]^{\dagger}$	σ	n	$\log \epsilon_{\odot}(X^{\dagger})$	σ	n	$\log \epsilon_{\odot}(X^{*})$	σ	n	$\log \epsilon_{\odot}(X_{\rm ASP09})$	σ	$\Delta \log \epsilon_{\odot}(X_1)$	$\log \epsilon_{\odot}(X_{\rm ASP21})$	σ	$\Delta \log \epsilon_{\odot}(X_2)$
	(dex)			(dex)			(dex)			(dex)		(dex)	(dex)		(dex)
C I	**0.14**	**0.22**	**2**	**8.48**	**0.11**	**2**	–	–	–	8.43	0.05	0.05	8.46	0.04	0.02
O I	**0.28**	**0.15**	**3**	**8.81**	**0.03**	**3**	–	–	–	8.69	0.05	0.12	8.69	0.04	0.12
Na I	-0.03	0.20	4	6.22	0.12	4	6.16	0.07	2	6.24	0.04	-0.02	6.22	0.03	0.00
Mg I	**0.24**	**0.16**	**5**	**7.62**	**0.03**	**5**	7.60	0.08	2	7.60	0.04	0.02	7.55	0.03	0.07
Mg II	–	–	–	**7.63**	**0.00**	**1**	–	–	–	7.60	0.04	0.03	7.55	0.03	0.08
Al I	**0.13**	**0.16**	**8**	**6.43**	**0.03**	**8**	–	–	–	6.45	0.03	-0.02	6.43	0.03	0.00
Si I	0.13	0.18	16	7.50	0.09	21	7.50	0.07	12	7.51	0.03	-0.01	7.51	0.03	-0.01
P I	–	–	–	**5.51**	**0.06**	**3**	–	–	–	5.41	0.03	0.10	5.41	0.03	0.10
S I	–	–	–	**7.15**	**0.00**	**2**	–	–	–	7.12	0.03	0.03	7.12	0.03	0.03
Ca I	0.15	0.20	15	6.29	0.09	21	6.34	0.08	18	6.34	0.04	-0.05	6.30	0.03	-0.01
Sc I	–	–	–	**3.13**	**0.00**	**1**	3.12	0.00	1	3.15	0.04	-0.02	3.14	0.04	-0.01
Sc II	0.06	0.14	2	3.14	0.02	12	3.23	0.08	7	3.15	0.04	-0.01	3.14	0.04	0.00
Ti I	0.21	0.21	44	4.93	0.09	63	4.96	0.09	43	4.95	0.05	-0.02	4.97	0.05	-0.04
Ti II	0.20	0.21	7	5.01	0.11	11	4.99	0.08	12	4.95	0.05	0.06	4.97	0.05	0.04
V I	**0.01**	**0.15**	**3**	**3.90**	**0.03**	**5**	3.99	0.05	5	3.93	0.08	-0.03	3.90	0.08	0.00
Cr I	-0.02	0.19	17	5.68	0.09	29	5.71	0.07	19	5.64	0.04	0.04	5.62	0.04	0.06
Cr II	0.01	0.20	3	5.64	0.11	4	5.64	0.14	3	5.64	0.04	0.00	5.62	0.04	0.02
Mn I	**-0.27**	**0.18**	**14**	**5.45**	**0.08**	**14**	5.62	0.13	13	5.43	0.05	0.02	5.42	0.06	0.03
Fe I	0.01	0.21	152	7.50	0.11	252	7.54	0.09	132	7.50	0.04	0.00	7.46	0.04	0.04
Fe II	0.00	0.20	17	7.50	0.09	32	7.51	0.04	17	7.50	0.04	0.00	7.46	0.04	0.04
Co I	**-0.10**	**0.17**	**6**	**4.95**	**0.06**	**8**	–	–	–	4.99	0.07	-0.04	4.94	0.05	0.01
Ni I	-0.02	0.20	45	6.25	0.10	66	6.28	0.09	54	6.22	0.04	0.03	6.20	0.04	0.05
Cu I	**-0.13**	**0.20**	**3**	**4.20**	**0.06**	**4**	–	–	–	4.19	0.04	0.01	4.18	0.05	0.02
Zn I	**0.20**	**0.15**	**2**	**4.63**	**0.02**	**2**	4.68	0.03	2	4.56	0.05	0.07	4.56	0.05	0.07
Sr I	**-0.18**	**0.14**	**1**	**2.84**	**0.00**	**1**	2.91	0.00	1	2.87	0.07	-0.03	2.83	0.06	0.01
Y II	**-0.14**	**0.15**	**2**	**2.28**	**0.02**	**2**	2.29	0.05	2	2.21	0.05	0.07	2.21	0.05	0.07
Zr I	–	–	–	2.53	0.00	1	–	–	–	2.58	0.04	-0.05	2.59	0.04	-0.06
Zr II	0.04	0.14	1	2.61	0.02	2	2.68	0.00	1	2.58	0.04	0.03	2.59	0.04	0.02
Ba II	**0.04**	**0.14**	**2**	**2.32**	**0.02**	**2**	2.24	0.06	4	2.18	0.09	0.14	2.27	0.05	0.05
La II	**0.03**	**0.16**	**2**	**1.14**	**0.05**	**3**	–	–	–	1.10	0.04	0.04	1.11	0.04	0.03
Ce II	**0.26**	**0.15**	**1**	**1.60**	**0.04**	**3**	1.64	0.02	2	1.58	0.04	0.02	1.58	0.04	0.02
Nd I	**0.08**	**0.15**	**1**	**1.36**	**0.03**	**3**	1.42	0.05	3	1.42	0.04	-0.06	1.42	0.04	-0.06
Sm II	**0.14**	**0.14**	**1**	**0.95**	**0.02**	**2**	0.96	0.00	1	0.96	0.04	-0.01	0.95	0.04	0.00

($\dagger$): This study, ($*$): Şahin et al. (2023), $\Delta \log \epsilon_{\odot}(X_1) = \log \epsilon_{\odot}(X^{\dagger}) - \log \epsilon_{\odot}(X_{\rm ASP09})$, $\Delta \log \epsilon_{\odot}(X_2) = \log \epsilon_{\odot}(X^{\dagger}) - \log \epsilon_{\odot}(X_{\rm ASP21})$

with the solar chemical abundances established by Asplund et al. (2009, 2021). The abundances of C, O, Mg, Al, P, S, Sc, Ti, V, Mn, Co, Cu, Zn, Sr, Y, Zr, Ba, La, Ce, Nd, and Sm reported in Table 2 were determined using both the equivalent width (EW) method and spectrum synthesis techniques. The synthetic spectra calculated for some sample lines (C I 9 111 Å, O I 7 772 Å, Mg I 5 711 Å, and Cu I 5 105 Å), whose elemental abundances were checked using the spectrum synthesis technique, are shown in Figure 4. On the other hand, when compared to the solar abundances reported by Asplund et al. (2009), the scatter among the elements ranges from -0.07 dex for Na to 0.16 dex for O. For the remaining 31 species, the average scatter in abundance ($\log \epsilon_{\odot}(X_{\rm ASP09})$) is 0.02±0.04 dex. Asplund et al. (2021) presented a revised solar chemical composition, with notable changes observed in the abundance of elements such as Ba, Mg, Co, Sr, Fe, and Ca. For instance, the abundance value obtained for Ba is 0.11 dex higher than that reported by Asplund et al. (2009) but shows better agreement with the values presented by Asplund et al. (2021). Similarly, a lower scatter was observed for Na compared to the results of Asplund et al. (2009).

The results can be affected by various systematic uncertainties, including those related to the correction of non-LTE effects on the formation of convection and atomic transitions. To investigate the potential convective effect, two different mixing length parameters (α) were calculated in this study using equations based on 2D hydrodynamic models from Ludwig et al. (1999) and 3D hydrodynamic models from Magic et al. (2015).

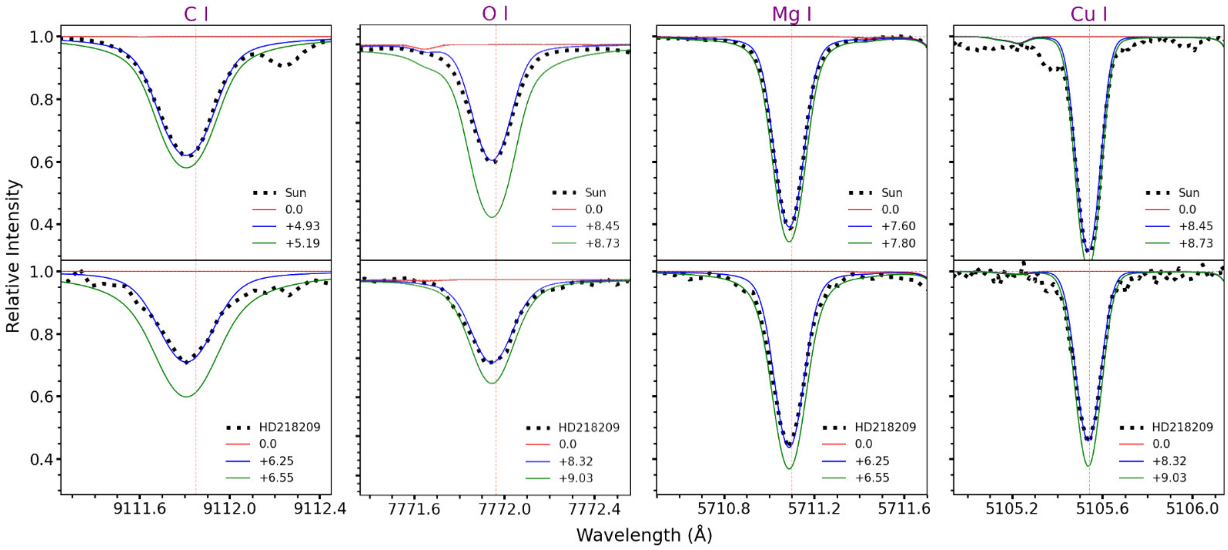

Figure 4. The figure presents observed (filled circles) and computed (full blue line) line profiles for C i 9 111 Å, O i 7 772 Å, Mg i 5 711 Å, and Cu i 5 105 Å in both the Sun (upper panels) and HD 218209 (bottom panels). The computed profiles represent the synthetic spectra derived from three logarithmic abundances. The red lines depict the spectra computed without considering the contributions from ionized metal lines.

The formula by Magic et al. (2015) yielded an α value of 1.99, whereas the formula by Ludwig et al. (1999) yielded an α value of 1.60. Two different ATLAS9 models were constructed for the two mixing-length parameters. The synthetic spectra calculated using these models were compared to the observed spectrum of HD 218209. Although no significant difference was observed, the synthetic spectrum derived from the mixing length parameter obtained by Magic et al. (2015) was found to be in slightly better agreement with the observed spectrum.

Given that the Fe i and Fe ii abundances were used to constrain the model atmospheric parameters in this study, we must consider the non-LTE effects on Fe. These effects were found to be negligible (0.00 dex) for both solar and stellar Fe ii lines (Bergemann et al. 2012a; Lind et al. 2012; Bensby et al. 2014). For Fe i lines with low excitation potentials (<8 eV) and metallicities [Fe/H] > -3.0 dex, the non-LTE deviations were minimal according to K (Lind et al. 2012). The non-LTE corrections (Bergemann et al. 2012b) for 66 Fe i lines in the IAG solar spectrum and 56 Fe i lines in HD 218209 were found to be 0.01 dex. Similar trends were observed for the other elements in both the Sun and Star. For example, the non-LTE corrections (Sun/Star) for Si i (-0.01/0.00), Ca i (-0.01/-0.01), Ti i (0.10/0.13), Ti ii (-0.01/0.00), Cr i (0.05/0.08), Mn i (0.05/0.12), and Co i (0.11/0.15) were generally small, with the largest corrections found for Ti and Co

3.1. Notes on the errors for model atmospheric parameters of the Sun

The solar spectrum is used as a standard reference spectrum for the spectroscopic analysis of F-G-K-type stars, in both the optical and NIR regions (Şahin & Bilir 2020; Şahin et al. 2023; Şentürk et al. 2024). This is mainly due to the well-characterized atmosphere of the Sun and extensive observational data in the optical and IR regions. Many published NIR line lists include lines with poorly defined or calibrated oscillator strengths, often relying on theoretical calculations (e.g., Ryde et al. 2009). In particular, a recent spectroscopic study of a solar analogue star, HD 76151, in the Y, J, H, and K bands by Şentürk et al. (2024) provides a detailed review of the line libraries published in the infrared region over the last 40 years in terms of $\log gf$ values and atomic data.

In the first paper of the series (Şahin et al. 2023), the effective temperature obtained from the solar atmosphere analysis differed by 20 K from the effective temperature value obtained in this study. This difference is consistent with the error values. Similarly, a significant difference in Paper I is the increase in the reported errors for $T_{\rm eff}$, $\log g$ because of the increase in the error for metallicity ($\Delta\sigma$[Fe/H] = 0.05 dex). For $T_{\rm eff}$, $\Delta\sigma T_{\rm eff}$ = 85 K and for $\log g$, $\Delta\sigma \log g$ = 0.10 cgs. In this study, we obtained an additional 187 atomic transitions in the near-IR region. In addition, two different solar spectra were preferred for the solar abundance analysis. The KPNO solar spectrum is in the 4 000-5 000 Å region and the IAG solar spectrum is in the 5 000-10 000 Å region.

The following subsections provide details of the line list and atomic data.

4. LINE LIST: IDENTIFICATION, LINE MEASUREMENT, AND ATOMIC DATA

Initially, the centers of the lines exhibiting Gaussian profiles appropriate for equivalent width analysis within the range of 4 000-10 000 Å were identified in the KPNO (Kurucz et al. 1984) and IAG solar spectra (Baker et al. 2020, BTFS). The established line centers for the selected isolated lines were compared with the wavelengths identified in the laboratory environment within the Revised Multiplet Table (RMT) (Moore et al. 1966). Subsequently, a multiplet (cf. Moore 1954) analysis technique was applied. The relative intensities of the lines within a multiplet are generally insensitive to variations in the excitation conditions in most spectroscopic sources. A standard approach involves verifying the presence of multiple members with expected relative intensities. Subsequent analyses focused on identifying lines that exhibited similar excitation and laboratory strengths.

The common wavelength range of the first article of the series and this study was 4 024-6 772 Å. In this range, 54 atomic transitions from 19 species of 17 elements were added to the first report on this series. The distributions of these transitions are Na I (one line), Al I (two lines), Si I (two lines), Ca I (two lines), Sc II (five lines), Ti I (four lines), V I (one line), Cr II (one line), Mn I (one line), Fe I (17 lines), Fe II (six lines), Co I (two lines), Cu I (two lines), Zr I (one line), Zr II (one line), La II (three lines), Ce II (one line), Nd II (one line) and Sm II (one line). In the region 6 772[8]-9 944 Å, 189 atomic transitions from 27 species of 23 elements were added to the line list. The distributions of these transitions are C I (two lines), O I (three lines), Na I (two lines), Mg I (three lines), Mg II (one line), AI I (eight lines), Si I (nine lines), P I (three lines), S I (two lines), Ca I (six lines), Sc II (five lines), Ti I (20 lines), V I (one line), Cr I (10 lines), Cr II (one line), Mn I (one line), Fe I (123 lines), Fe II (15 lines), Co I (three lines), Ni I (13 lines), Cu I (four lines), Zr I (one line), Zr II (one line), La II (three lines), Ce II (one line), Nd I (two lines), and Sm II (one line). In total, 13 atomic transitions from seven species of seven elements were included in the first article of the series but were not included in this study. The statistics of these transitions are as follows: Ca I (three lines), Ti II (one line), Fe I (three lines), Co I (two lines), Ni I (one line), Zr II (one line), and Nd II (two lines). Lower-level excitation potential (L.E.P) values for the new line list were obtained from the MOORE catalogue (Moore et al. 1966).

Accurate determination of elemental abundances in stars requires precise knowledge of the atomic transition probability, quantified by the $\log gf$ value. This study utilized a comprehensive compilation of $\log gf$ values from recent literature, including Biemont & Godefroid (1980); Biemont et al. (1981), Hannaford et al. (1982), Klose et al. (2002), Takeda et al. (2003), Fuhr & Wiese (2006), Kelleher & Podobedova (2008), Lawler et al. (2009), Den Hartog et al. (2011), Shi et al. (2011), Hansen et al. (2013), Lawler et al. (2006, 2013, 2015, 2017, 2019), Pehlivan Rhodin et al. (2017), and Den Hartog et al. (2021). For transitions not documented in these sources, data from the NIST[9] and VALD[10] atomic line databases were used. When multiple sources were available, the $\log gf$ value that yielded the most consistent abundance with solar abundance

[8] Upper wavelength limit from Şahin et al. (2023) is 6 780 Å.
[9] http://physics.nist.gov/PhysRefData/ASD
[10] https://vald.astro.uu.se/

Table 3. Comparison of $\log gf$ values for common lines in GESv6. The number of common lines (n) was also reported. The mean of the $\log gf$ differences ($\Delta \log gf$) for each element is also reported.

Element	n	$\Delta\log(gf)$ (dex)	σ (dex)	Element	n	$\Delta\log(gf)$ (dex)	σ (dex)
C I	2	-0.02	0.02	Mn I	12	0.68	0.83
O I	3	0.00	0.00	Fe I	236	0.00	0.16
Na I	4	0.01	0.02	Fe II	28	0.00	0.07
Mg I	5	0.32	0.54	Co I	7	1.33	1.03
Mg II	1	-0.01	0.00	Ni I	66	-0.04	0.10
Al I	8	0.29	0.58	Cu I	4	0.27	0.26
Si I	19	-0.01	0.11	Zn I	2	-0.03	0.02
S I	2	-0.29	0.24	Sr I	1	0.00	0.00
Ca I	20	0.00	0.04	Y II	2	-0.07	0.05
Sc II	12	0.02	0.06	Zr I	1	0.00	0.00
Ti I	56	0.00	0.03	Ba II	2	-0.02	0.01
Ti II	11	0.04	0.11	La II	2	-0.01	0.01
V I	5	0.71	0.61	Ce II	2	0.00	0.00
Cr I	26	0.07	0.49	Nd II	2	0.00	0.00
Cr II	4	0.12	0.20	Sm II	2	0.00	0.00

$\Delta\log(gf) = \log(gf)_{\text{This Study}} - \log(gf)_{\text{GESv6}}$

values reported by Asplund et al. (2009, 2021) was prioritized. References for the adopted $\log gf$ values and corresponding RMT numbers for each line are tabulated in Tables A1, A2, A3, A4, and A5.

Further verification of the $\log gf$ values was performed by comparing the $\log gf$ values used in this study with those in the *Gaia*-ESO line list v.6 provided by GES collaboration (Heiter et al. 2021). Note that the gf values for the chosen lines of Fe I and Fe II in this study were obtained from Fuhr & Wiese (2006). The GES line list contains the recommended lines and atomic data (i.e., gf values corrected for the hyperfine structure) for the analysis of FGK stars. Notably, several lines in the spectra of FGK stars have not yet been identified (Heiter et al. 2015).

The GES line list (v.6) comprises 141 233 lines spanning a 4 200-9 200Å. A total of 561 lines were analyzed in this study, of which 548 were common to the GES line list. These 592 atomic transitions involve 30 species from 26 elements. A total of 40 atomic transitions were included in this study's line list in the regions outside the GES line list boundaries (lower limit: 4 021-4 200 Å and upper limit: 9 200-9 944 Å). In the spectral region overlapping with the GES line list (4 200-9 200 Å), additional Fe I (8958.88 Å), and Fe II (6806.85 Å, 6810.28 Å, 6820.43 Å) atomic transitions were found compared to the GES line list. Of the 55 lines identified in this study within the same wavelength range, 51 were found in the GES line list. This wavelength range aligns with the PolarBASE spectrum of HD 218209 used in this analysis.

For the 236 common Fe I lines in the GES line list, the difference in the $\log gf$ value was 0.00 ± 0.16 dex. For the 28 Fe II lines, the difference in the $\log gf$ values was 0.00 ± 0.07 dex. A detailed comparison of the $\log gf$ values was performed for the 548 lines common to both line lists, as listed in Table 3 which summarises the mean difference in log gf values and

the corresponding standard deviations for each element with at least two common lines. The results show overall good agreement between the two line lists, though significant differences were observed for certain elements, such as Co and Mn. These discrepancies can be attributed to various factors including differences in the atomic data used to construct the line lists, uncertainties in the line identification process, and the presence of non-LTE effects.

Figure 5 presents the numerical statistics for the final line list generated in this study are shown in Figure 5. The same figure shows the number of lines in the spectral region of 50 Å each.

5. CONCLUSION

This study presents an expanded line list covering the wavelength range of 4 080–10 000 Å for abundance analyses of F- and G-type stars. Although Paper I reported 363 atomic transitions, only 592 lines were reported in this study. The line list was compared with the existing *Gaia*-ESO v6 line list (Table 3), and a 93% overlap was found, with 548 of the 592 line matches.

Utilizing high-resolution solar spectra from IAG (5 000-10 000 Å, R ≈1 000 000) and KPNO (4 000-6 780 Å, R≈700 000), 592 spectral lines belonging to 33 chemical species were identified and included in the abundance analysis. Compared to the previous paper in this series, not only has the wavelength range extended, but elements such as C, O, Al, P, S, Co, Cu, Zr, and La have also been added to the list.

Additionally, the abundances of C, O, Mg, Al, P, S, Sc, V, Mn, Co, Cu, Zn, Sr, Y, Zr, Ba, La, Ce, Nd, and Sm were determined using the synthesis method. To calculate the reported abundances, it was assumed that the solar spectrum was disk-integrated[11].

A comparison of the elemental abundances ([X/Fe]) reported in this study for HD 218209 with those presented by (Şahin et al. 2023) reveals several differences. No significant differences were observed for Cr II, Ti I, V I, Sr I, and Zr II ($\Delta \log_\epsilon$ = 0.00 dex). Elements exhibiting a difference of -0.01 dex include Fe I, Ni I, Cr I, Ca I, and Nd II. A difference of 0.06 dex was observed for Ce II, Ba II, and Sc II. Other notable differences include -0.02 dex for Na I and Ti II, 0.01 dex for Si I, 0.07 dex for Y II, 0.05 dex for Mn I, 0.02 dex for Zn I, 0.09 dex for Co I, and 0.04 dex for Mg I.

In this study, we employed both equivalent width (EW) measurements and spectrum synthesis techniques to determine the elemental abundances in the solar and HD 218209 spectra. The resulting abundances were compared to those reported by Asplund et al. (2009) and Asplund et al. (2021) as well as other solar abundance values found in the literature (Table A6). Our results are in excellent agreement with those of the previous studies. Notably, the revision of Ba abundance in Asplund et al. (2021) significantly reduced the discrepancy between the two studies.

Having accurately determined the solar abundances using a constructed line list, we applied a similar methodology to the star, HD 218209. Table A7 presents a comparison of the effective temperature, surface gravity, metallicity, and derived chemical abundances of this star. A thorough examination of the available abundance data for HD 218209 revealed a scarcity of literature regarding the abundance of several elements (C, O, Cr, Co, Cu, Zn, Sr, Y, Zr, Ba, La, Ce, Nd, and Sm). This highlights the significant contributions of our study to this field. A detailed element-by-element literature analysis is provided in Appendix A1.

[11] At this point, the flux/int switch in the abfind and synth drivers of the MOOG code, which we used to determine model atmosphere parameters and abundance calculations under LTE conditions, was set to zero.

Peer Review: Externally peer-reviewed.

Author Contribution: Conception/Design of study - T.Ş.; Data Acquisition - T.Ş., F.G., M.M., S.A.Ş; Data Analysis/Interpretation - T.Ş., F.G., S.A.Ş., M.M., N.Ç.; Drafting Manuscript - T.Ş.; Critical Revision of Manuscript - T.Ş.; Final Approval and Accountability - T.Ş., F.G., S.A.Ş., M.M., N.Ç.; Technical or Material - T.Ş., M.M., F.G.; Support Supervision - T.Ş.

Conflict of Interest: Authors declared no conflict of interest.

Financial Disclosure: This study was supported by the Scientific and Technological Research Council of Turkey (TUBITAK) under Grant Number 121F265. The authors thank TUBITAK for their support.

Acknowledgements: This study used NASA's Astrophysics Data System and the SIMBAD database operated at CDS, Strasbourg, France. The nonpublic data underlying this article will be made available upon reasonable request from the authors.

Software: LIME (Şahin 2017), SPECTRE (Sneden 1973), MOOG (Sneden 1973)

LIST OF AUTHOR ORCIDS

T. Şahin	https://orcid.org/0000-0002-0296-233X
F. Güney	https://orcid.org/0000-0003-3884-974X
S.A. Şentürk	https://orcid.org/0000-0003-3863-6525
N. Çınar	https://orcid.org/0000-0002-5155-9280
M. Marışmak	https://orcid.org/0000-0002-9397-2778

REFERENCES

Abia C., Rebolo R., Beckman J. E., Crivellari L., 1988, A&A, 206, 100

Aoki W., Matsuno T., Parthasarathy M., 2022, PASJ, 74, 1368

Asplund M., Grevesse N., Sauval A. J., Scott P., 2009, ARA&A, 47, 481

Asplund M., Amarsi A. M., Grevesse N., 2021, A&A, 653, A141

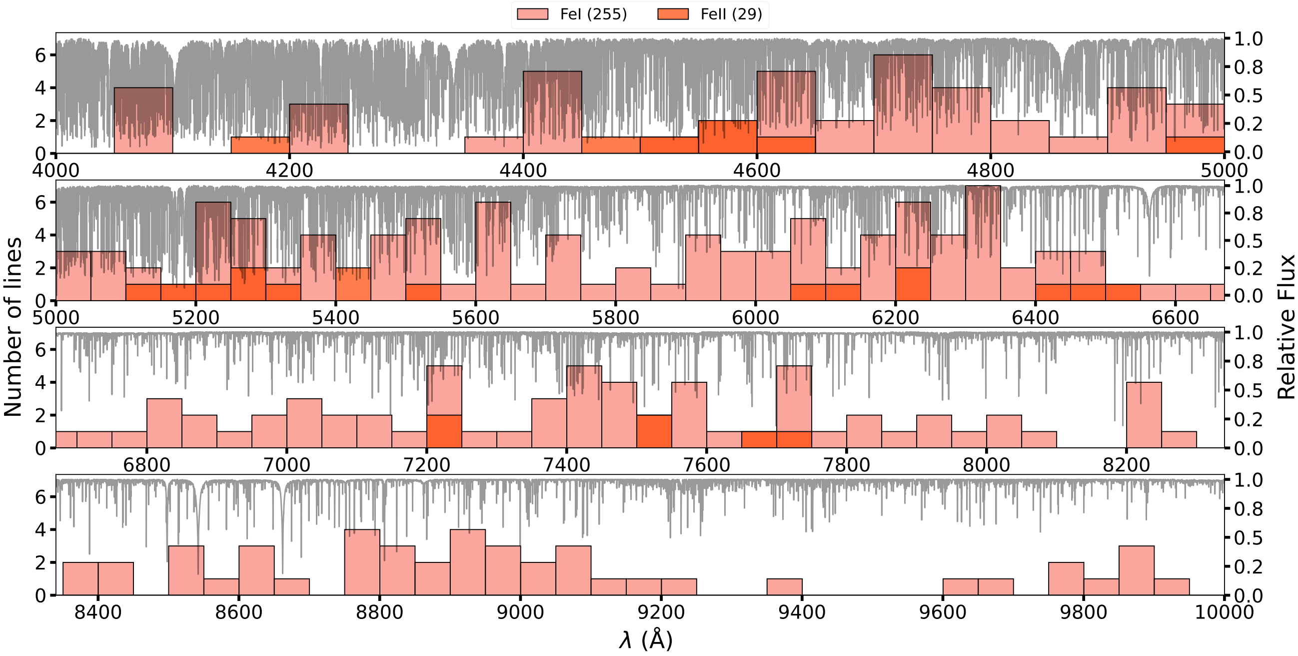

Figure 5. The figure displays the telluric-free Solar spectrum obtained from Baker et al. (2020), along with the number of identified lines within each 50 Å region of the spectrum. The 4 000 - 5 000 Å spectral range is based on solar data from Kurucz et al. (1984), while the 5 000 - 10 000 Å range utilizes the telluric-free Solar spectrum (BTFS) provided by Baker et al. (2020).

Baker A. D., Blake C. H., Reiners A., 2020, ApJS, 247, 24

Bensby T., Feltzing S., Lundström I., 2003, A&A, 410, 527

Bensby T., Feltzing S., Oey M. S., 2014, A&A, 562, A71

Bergemann M., Lind K., Collet R., Magic Z., Asplund M., 2012a, MNRAS, 427, 27

Bergemann M., Kudritzki R.-P., Plez B., Davies B., Lind K., Gazak Z., 2012b, ApJ, 751, 156

Biemont E., Godefroid M., 1980, A&A, 84, 361

Biemont E., Grevesse N., Hannaford P., Lowe R. M., 1981, ApJ, 248, 867

Biemont E., Hibbert A., Godefroid M., Vaeck N., 1993, ApJ, 412, 431

Caffau E., Steffen M., Sbordone L., Ludwig H. G., Bonifacio P., 2007, A&A, 473, L9

Caffau E., Ludwig H. G., Steffen M., Ayres T. R., Bonifacio P., Cayrel R., Freytag B., Plez B., 2008, A&A, 488, 1031

Caffau E., Maiorca E., Bonifacio P., Faraggiana R., Steffen M., Ludwig H. G., Kamp I., Busso M., 2009, A&A, 498, 877

Caffau E., Ludwig H. G., Bonifacio P., Faraggiana R., Steffen M., Freytag B., Kamp I., Ayres T. R., 2010, A&A, 514, A92

Caffau E., Ludwig H. G., Steffen M., Freytag B., Bonifacio P., 2011, Sol. Phys., 268, 255

Caffau E., et al., 2019, A&A, 622, A68

Castelli F., Kurucz R. L., 2003, in Piskunov N., Weiss W. W., Gray D. F., eds, IAU Symposium Vol. 210, Modelling of Stellar Atmospheres. p. A20 (arXiv:astro-ph/0405087), doi:10.48550/arXiv.astro-ph/0405087

Den Hartog E. A., Lawler J. E., Sobeck J. S., Sneden C., Cowan J. J., 2011, ApJS, 194, 35

Den Hartog E. A., Lawler J. E., Sneden C., Cowan J. J., Roederer I. U., Sobeck J., 2021, ApJS, 255, 27

Fuhr J. R., Wiese W. L., 2006, Journal of Physical and Chemical Reference Data, 35, 1669

Gehren T., Liang Y. C., Shi J. R., Zhang H. W., Zhao G., 2004, A&A, 413, 1045

Grevesse N., Asplund M., Sauval A. J., 2007, Space Sci. Rev., 130, 105

Hannaford P., Lowe R. M., Grevesse N., Biemont E., Whaling W., 1982, ApJ, 261, 736

Hansen C. J., Bergemann M., Cescutti G., François P., Arcones A., Karakas A. I., Lind K., Chiappini C., 2013, A&A, 551, A57

Haywood M., 2008, A&A, 482, 673

Heiter U., et al., 2015, Phys. Scr., 90, 054010

Heiter U., et al., 2021, A&A, 645, A106

Holweger H., 2001, in Wimmer-Schweingruber R. F., ed., American Institute of Physics Conference Series Vol. 598, Joint SOHO/ACE workshop "Solar and Galactic Composition". AIP, pp 23–30 (arXiv:astro-ph/0107426), doi:10.1063/1.1433974

Karathanou K., Kemmler L., Lazaratos M., Siemers M., Bondar A.-N., 2020, Biophysical Journal, 118, 179a

Kelleher D. E., Podobedova L. I., 2008, Journal of Physical and Chemical Reference Data, 37, 1285

Klose J. Z., Fuhr J. R., Wiese W. L., 2002, Journal of Physical and Chemical Reference Data, 31, 217

Kurucz R. L., Furenlid I., Brault J., Testerman L., 1984, Solar flux atlas from 296 to 1300 nm

Lambert D. L., 1978, MNRAS, 182, 249

Lawler J. E., Den Hartog E. A., Sneden C., Cowan J. J., 2006, ApJS, 162, 227

Lawler J. E., Sneden C., Cowan J. J., Ivans I. I., Den Hartog E. A., 2009, ApJS, 182, 51

Lawler J. E., Guzman A., Wood M. P., Sneden C., Cowan J. J., 2013, ApJS, 205, 11

Lawler J. E., Sneden C., Cowan J. J., 2015, ApJS, 220, 13

Lawler J. E., Sneden C., Nave G., Den Hartog E. A., Emrahoğlu N., Cowan J. J., 2017, ApJS, 228, 10

Lawler J. E., Hala Sneden C., Nave G., Wood M. P., Cowan J. J., 2019, ApJS, 241, 21

Lind K., Bergemann M., Asplund M., 2012, Monthly Notices of the Royal Astronomical Society, 427, 50

Lodders K., 2003, ApJ, 591, 1220

Lodders K., Palme H., Gail H. P., 2009, Landolt Börnstein, 4B, 712

Luck R. E., 2017, AJ, 153, 21

Ludwig H.-G., Freytag B., Steffen M., 1999, A&A, 346, 111

Magic Z., Weiss A., Asplund M., 2015, A&A, 573, A89

Marışmak M., Şahin T., Güney F., Plevne O., Bilir S., 2024, Astronomische Nachrichten, 345, e20240047

Mishenina T. V., Soubiran C., Kovtyukh V. V., Korotin S. A., 2004, A&A, 418, 551

Mishenina T. V., Gorbaneva T. I., Basak N. Y., Soubiran C., Kovtyukh V. V., 2011, Astronomy Reports, 55, 689

Mishenina T. V., Pignatari M., Korotin S. A., Soubiran C., Charbonnel C., Thielemann F. K., Gorbaneva T. I., Basak N. Y., 2013, A&A, 552, A128

Molaro P., Monai S., 2012, A&A, 544, A125

Moore C. E., 1954, Science, 119, 449

Moore C. E., Minnaert M. G. J., Houtgast J., 1966, The Solar Spectrum 2935 Å to 8770 Å: Second Revision of Rowland's Preliminary Table of Solar Spectrum Wavelengths. Vol. 61, National Bureau of Standards

Ofman L., Yogesh Giordano S., 2024, ApJ, 970, L16

Pagel B. E. J., Patchett B. E., 1975, MNRAS, 172, 13

Pehlivan Rhodin A., Hartman H., Nilsson H., Jönsson P., 2017, A&A, 598, A102

Petit P., Louge T., Théado S., Paletou F., Manset N., Morin J., Marsden S. C., Jeffers S. V., 2014, PASP, 126, 469

Rice M., Brewer J. M., 2020, ApJ, 898, 119

Ryde N., Edvardsson B., Gustafsson B., Eriksson K., Käufl H. U., Siebenmorgen R., Smette A., 2009, A&A, 496, 701

Şahin T., 2017, Turkish Journal of Physics, 41, 367

Şahin T., Bilir S., 2020, ApJ, 899, 41

Şahin T., Lambert D. L., 2009, MNRAS, 398, 1730

Şahin T., Lambert D. L., Klochkova V. G., Tavolganskaya N. S., 2011, MNRAS, 410, 612

Şahin T., Lambert D. L., Klochkova V. G., Panchuk V. E., 2016, MNRAS, 461, 4071

Şahin T., Marismak M., Cinar N., Bilir S., 2023, Physics and Astronomy Reports, 1, 54

Salmon S. J. A. J., Van Grootel V., Buldgen G., Dupret M. A., Eggenberger P., 2021, A&A, 646, A7

Şentürk S. A., Şahin T., Güney F., Bilir S., Marışmak M., 2024, ApJ, 976, 175

Sharma S., et al., 2018, MNRAS, 473, 2004

Shi J. R., Gehren T., Zhao G., 2011, A&A, 534, A103

Sneden C. A., 1973, PhD thesis, University of Texas, Austin

Takeda Y., 2023, Acta Astron., 73, 35

Takeda Y., Zhao G., Takada-Hidai M., Chen Y.-Q., Saito Y.-J., Zhang H.-W., 2003, Chinese J. Astron. Astrophys., 3, 316

Takeda Y., Kawanomoto S., Honda S., Ando H., Sakurai T., 2007, A&A, 468, 663

Trevisan M., Mamon G. A., Thuan T. X., Ferrari F., Pilyugin L. S., Ranjan A., 2021, MNRAS, 502, 4815

Valenti J. A., Fischer D. A., 2005, ApJS, 159, 141

Wang Y., Zhao G., 2013, ApJ, 769, 4

Woolf V. M., West A. A., 2012, MNRAS, 422, 1489

Zhang W. W., et al., 2019, in O'Dell S. L., Pareschi G., eds, Society of Photo-Optical Instrumentation Engineers (SPIE) Conference Series Vol. 11119, Optics for EUV, X-Ray, and Gamma-Ray Astronomy IX. p. 1111907, doi:10.1117/12.2530284

da Silva R., Milone A. d. C., Rocha-Pinto H. J., 2015, A&A, 580, A24

APPENDIX A: APPENDIX

A1. Literature Review for HD 218209

This section presents a comprehensive literature review of the elemental abundances of the star, focusing on studies conducted over the past four decades. Table A7 summarizes the literature values for each element and compares our results with those of previous studies.

Carbon abundance for star has been reported in the literature over the last decade by da Silva et al. (2015, DA15), Rice & Brewer (2020, RI20), and Takeda (2023, TA23). The carbon abundance ([C/Fe]=0.14 dex) reported in this study is in good agreement with that of Rice & Brewer (2020, RI20) ([C/Fe]=0.18 dex), differing by only 0.04 dex. The largest discrepancy is found for Takeda (2023, TA23), with a difference of 0.22 dex.

The literature values for [O/Fe] exhibited a scatter of approximately 0.3 dex. Our value ($\approx$ 0.3 dex) agrees well with Mishenina et al. (2013, MI13) (Δ = 0.06 dex), but shows a larger discrepancy than Takeda (2023, TA23) (Δ = 0.20 dex) and Rice & Brewer (2020, RI20) (Δ = 0.14 dex).

The [Na/Fe] ratio of -0.03 dex shows good agreement with Mishenina et al. (2011, MI11) ($\Delta = -0.01$ dex), Rice & Brewer (2020, RI20) ($\Delta = -0.06$ dex), Luck (2017, LU17) ($\Delta = -0.09$ dex), and Valenti & Fischer (2005, VA05) ($\Delta = -0.13$ dex). However, a significant discrepancy ($\Delta = -0.26$ dex) was observed compared to in that Gehren et al. (2004, GE04).

Moving on to magnesium, our [Mg/Fe] value of 0.24 dex is consistent with the values reported in Mishenina et al. (2004, MI04), Mishenina et al. (2013, MI13) (Δ = 0.05 dex), da Silva et al. (2015, DA15) (Δ = 0.06 dex), Rice & Brewer (2020, RI20) (Δ = 0.07 dex), and Luck (2017, LU17) ($\Delta = -0.05$ dex). However, a significant discrepancy of -0.17 dex was observed compared to Gehren et al. (2004, GE04).

The reported [Al/Fe] ratio in this study is consistent with the values reported by Mishenina et al. (2011, MI11), da Silva et al. (2015, DA15), Luck (2017, LU17), and Rice & Brewer (2020, RI20), except for the abundance ratio reported by Abia et al. (1988, AB88), which shows a significant discrepancy ($\Delta = -0.32$ dex).

The literature values for [Si/Fe] exhibited a relatively homogeneous distribution. Our value of 0.13 dex agrees well with da Silva et al. (2015, DA15) and Luck (2017, LU17) (Δ = 0.02 dex). The largest discrepancy was observed in Takeda et al. (2007, TA07) (Δ = −0.13 dex).

Our [Ca/Fe] value of 0.15 dex is in good agreement with Rice & Brewer (2020, RI20) (Δ = 0.03 dex), da Silva et al. (2015, DA15) (Δ = 0.02 dex), and Luck (2017, LU17) (Δ = −0.04 dex). A significant discrepancy is observed with Mishenina et al. (2011, MI11) (Δ = 0.50 dex).

Our [Sc/Fe] value of 0.06 dex shows a discrepancy of 0.09 dex compared to Luck (2017, LU17).

Our [Ti/Fe] value of 0.21 dex agrees well with Luck (2017, LU17) and shows good agreement with da Silva et al. (2015, DA15) (Δ = 0.01 dex), Valenti & Fischer (2005, VA05) (Δ = −0.02 dex), and Rice & Brewer (2020, RI20) (Δ = −0.03 dex). A significant discrepancy is observed with Takeda et al. (2007, TA07) (Δ = 0.18 dex).

Our [V/Fe] value of -0.02 dex aligns well with the findings of Takeda et al. (2007, TA07) (Δ = 0.05 dex) but shows discrepancies of 0.19 dex, 0.18 dex, and 0.15 dex when compared to Rice & Brewer (2020, RI20), Luck (2017, LU17), and da Silva et al. (2015, DA15), respectively.

The [Cr/Fe] value determined in this study agrees well with previous findings, with discrepancies of approximately ±0.05 dex observed when compared to Rice & Brewer (2020, RI20) and Luck (2017, LU17).

Our [Mn/Fe] value of -0.27 dex precisely matches the value reported by Rice & Brewer (2020, RI20) and demonstrates good agreement with da Silva et al. (2015, DA15) (Δ = −0.09 dex) and Luck (2017, LU17) (Δ = −0.03 dex).

The [Co/Fe] value determined in this study exhibits discrepancies of -0.18 dex compared to Luck (2017, LU17) and -0.23 dex compared to Takeda et al. (2007, TA07).

The [Ni/Fe] value determined in this study aligns well with the literature values, with the exception of a significant discrepancy (Δ = −0.21 dex) observed in the work of Abia et al. (1988, AB88). The smallest discrepancy is found with Luck (2017, LU17) (Δ = −0.01 dex), followed by Rice & Brewer (2020, RI20) (Δ = −0.03 dex), Mishenina et al. (2013, MI13) and Mishenina et al. (2004, MI04) (Δ = −0.06 dex), and Takeda et al. (2007, TA07) (Δ = −0.02 dex).

The [Cu/Fe] value determined in this study shows discrepancies of -0.10 dex compared to Luck (2017, LU17), -0.06 dex compared to da Silva et al. (2015, DA15), and -0.11 dex compared to Mishenina et al. (2011, MI11).

The [Zn/Fe] value determined in this study is in good agreement with literature values, with a difference of 0.08 dex compared to Luck (2017, LU17) and 0.06 dex compared to Mishenina et al. (2013, MI13).

The [Sr/Fe] value of 0.10 dex determined in this study exhibits a discrepancy of -0.28 dex compared to Luck (2017, LU17).

The [Y/Fe] value determined in this study shows discrepancies of -0.16 dex compared to Rice & Brewer (2020, RI20), -0.22 dex compared to Luck (2017, LU17), and -0.10 dex compared to Mishenina et al. (2011, MI11).

The [Zr/Fe] value determined in this study agrees well with Mishenina et al. (2013, MI13) (Δ = 0.04 dex), but shows a discrepancy of -0.21 dex compared to Luck (2017, LU17).

The [Ba/Fe] value determined in this study precisely matches that reported by Luck (2017, LU17) ([Ba/Fe]=0.04 dex), while a difference of 0.03 dex is observed compared to Mishenina et al. (2013, MI13).

The [La/Fe] value determined in this study shows a discrepancy of -0.60 dex compared to Luck (2017, LU17), while a difference of -0.06 dex is observed compared to Mishenina et al. (2013, MI13).

The [Ce/Fe] value determined in this study shows a discrepancy of -0.02 dex compared to Luck (2017, LU17), while a difference of -0.28 dex is observed compared to Mishenina et al. (2013, MI13).

The difference in neodymium abundance compared to Luck (2017, LU17) is -0.24 dex, while the difference compared to Mishenina et al. (2013, MI13) is -0.07 dex.

The [Sm/Fe] value determined in this study shows a discrepancy of -0.12 dex compared to Luck (2017, LU17), while a difference of 0.01 dex is observed compared to Mishenina et al. (2013, MI13).

Table A1. Fe I and Fe II lines. The abundances were obtained for a model with T_{eff} = 5770 K, log g = 4.40 cgs, and ξ = 0.66 km s^{-1} for the solar spectrum. T_{eff} =5600 K, log g = 4.50 cgs, and ξ = 0.44 km s^{-1} for the HD 218209 spectrum.

Spec.	λ (Å)	LEP (eV)	log(gf) (dex)	Sun EW (mÅ)	Sun log ϵ(X) (dex)	HD 218209 EW (mÅ)	HD 218209 log ϵ(X) (dex)	RMT	Ref.	Spec.	λ (Å)	LEP (eV)	log(gf) (dex)	Sun EW (mÅ)	Sun log ϵ(X) (dex)	HD 218209 EW (mÅ)	HD 218209 log ϵ(X) (dex)	RMT	Ref.
Fe I	4080.22	3.28	-1.23	80.9	7.32	-	-	558	1	Fe I	5501.48	0.96	-3.05	115.3	7.50	104.5	7.08	15	1
Fe I	4082.11	3.42	-1.51	68.2	7.49	-	-	698	1	Fe I	5506.79	0.99	-2.80	123.2	7.37	111.4	6.94	15	1
Fe I	4088.56	3.64	-1.50	52.3	7.41	-	-	906	1	Fe I	5525.55	4.23	-1.08	53.0	7.35	39.4	6.96	1062	1
Fe I	4090.96	3.37	-1.73	55.8	7.37	-	-	695	1	Fe I	5543.94	4.22	-1.11	61.5	7.55	49.1	7.17	1062	1
Fe I	4204.00	2.84	-1.01	125.1	7.50	-	-	355	1	Fe I	5546.51	4.37	-1.28	50.8	7.63	35.9	7.21	1145	1
Fe I	4207.13	2.83	-1.41	82.5	7.39	77.3	7.12	352	1	Fe I	5560.22	4.43	-1.16	50.2	7.55	36.4	7.15	1164	1
Fe I	4220.35	3.07	-1.31	83.6	7.46	77.4	7.16	482	1	Fe I	5618.64	4.21	-1.28	50.0	7.47	36.1	7.06	1107	1
Fe I	4365.90	2.99	-2.25	51.4	7.48	40.7	7.09	415	1	Fe I	5624.03	4.39	-1.20	50.4	7.56	37.2	7.18	1160	1
Fe I	4432.58	3.57	-1.56	51.9	7.37	42.9	7.04	797	1	Fe I	5633.95	4.99	-0.32	65.3	7.57	53.3	7.23	1314	1
Fe I	4439.89	2.28	-3.00	52.1	7.56	36.7	7.03	116	1	Fe I	5636.71	3.64	-2.56	20.7	7.53	13.6	7.18	868	1
Fe I	4442.35	2.20	-1.25	187.7	7.52	-	-	68	1	Fe I	5638.27	4.22	-0.84	76.6	7.53	67.7	7.23	1087	1
Fe I	4447.14	2.20	-2.73	66.6	7.64	57.3	7.27	69	1	Fe I	5641.45	4.26	-1.15	66.7	7.70	49.0	7.24	1087	1
Fe I	4447.73	2.22	-1.34	171.0	7.52	-	-	68	1	Fe I	5662.52	4.18	-0.57	91.2	7.57	81.4	7.25	1087	1
Fe I	4502.60	3.57	-2.31	28.6	7.50	-	-	796	1	Fe I	5701.56	2.56	-2.22	84.8	7.61	72.7	7.21	209	1
Fe I	4556.93	3.25	-2.66	26.8	7.49	-	-	638	1	Fe I	5705.47	4.30	-1.36	37.8	7.37	25.4	6.98	1087	1
Fe I	4593.53	3.94	-2.03	28.3	7.53	-	-	971	1	Fe I	5717.84	4.28	-1.10	62.1	7.58	-	-	1107	1
Fe I	4602.01	1.61	-3.15	70.9	7.53	63.9	7.20	39	1	Fe I	5741.86	4.26	-1.67	32.6	7.52	-	-	1086	1
Fe I	4602.95	1.48	-2.22	118.8	7.44	110.7	7.06	39	1	Fe I	5778.46	2.59	-3.43	22.4	7.42	15.5	7.06	209	1
Fe I	4619.30	3.60	-1.08	83.9	7.43	68.9	6.98	821	1	Fe I	5806.73	4.61	-1.03	51.6	7.58	41.9	7.28	1180	1
Fe I	4630.13	2.28	-2.59	73.2	7.62	66.5	7.29	115	1	Fe I	5814.80	4.26	-1.94	22.0	7.53	12.2	7.10	1086	1
Fe I	4635.85	2.84	-2.36	54.1	7.50	42.5	7.08	349	1	Fe I	5881.28	4.59	-1.70	14.3	7.35	-	-	1178	1
Fe I	4661.54	4.54	-1.26	37.9	7.54	25.1	7.14	1207	1	Fe I	5905.67	4.63	-0.77	57.0	7.44	-	-	1181	1
Fe I	4678.85	3.60	-0.83	syn	7.54	syn	7.06	821	1	Fe I	5916.26	2.45	-2.99	54.4	7.60	45.2	7.26	170	1
Fe I	4704.95	3.69	-1.53	62.7	7.56	53.5	7.22	821	1	Fe I	5929.68	4.55	-1.38	39.5	7.65	24.8	7.21	1176	1
Fe I	4728.55	3.65	-1.17	81.3	7.63	-	-	822	1	Fe I	5934.67	3.93	-1.12	76.0	7.44	59.8	7.01	982	1
Fe I	4733.60	1.48	-2.99	83.9	7.58	77.8	7.26	38	1	Fe I	5952.73	3.98	-1.39	59.6	7.48	-	-	959	1
Fe I	4735.85	4.07	-1.32	64.1	7.77	-	-	1042	1	Fe I	5956.71	0.86	-4.61	50.9	7.55	44.4	7.23	14	1
Fe I	4741.53	2.83	-1.76	71.3	7.36	66.0	7.11	346	1	Fe I	5983.70	4.53	-0.49	67.1	7.35	57.5	7.04	1175	3
Fe I	4745.81	3.65	-1.27	73.9	7.59	68.3	7.32	821	1	Fe I	6003.03	3.86	-1.03	81.3	7.38	72.4	7.06	959	2
Fe I	4779.44	3.40	-2.02	40.7	7.34	-	-	720	1	Fe I	6005.53	2.58	-3.60	21.8	7.56	15.8	7.23	959	3
Fe I	4788.77	3.24	-1.76	65.4	7.58	-	-	588	1	Fe I	6027.06	4.07	-1.09	63.5	7.47	-	-	1018	1
Fe I	4793.96	3.03	-3.47	8.7	7.43	-	-	512	1	Fe I	6065.49	2.61	-1.53	117.0	7.41	-	-	207	1
Fe I	4794.36	2.41	-4.05	11.5	7.55	-	-	115	2	Fe I	6078.50	4.77	-0.32	75.9	7.53	62.3	7.16	1259	3
Fe I	4802.89	3.64	-1.51	59.7	7.49	47.6	7.10	888	1	Fe I	6079.02	4.65	-1.10	44.4	7.55	28.9	7.12	1176	1
Fe I	4839.55	3.27	-1.82	61.8	7.57	55.8	7.32	588	1	Fe I	6082.72	2.22	-3.57	34.3	7.48	24.1	7.08	64	1
Fe I	4875.88	3.33	-1.97	61.0	7.58	-	-	687	1	Fe I	6096.67	3.98	-1.88	36.9	7.53	24	7.12	959	1
Fe I	4917.23	4.19	-1.16	62.8	7.60	51.9	7.25	1066	1	Fe I	6127.91	4.14	-1.40	47.5	7.49	36.8	7.15	1017	1
Fe I	4918.02	4.23	-1.34	52.0	7.60	40.0	7.23	1070	1	Fe I	6137.70	2.59	-1.40	129.4	7.40	114.3	6.98	207	1
Fe I	4924.78	2.28	-2.11	92.6	7.50	85.5	7.16	114	1	Fe I	6157.73	4.07	-1.22	61.5	7.55	48.8	7.17	1015	1
Fe I	4939.69	0.86	-3.34	98.4	7.53	-	-	16	1	Fe I	6165.36	4.14	-1.47	43.9	7.48	30.5	7.07	1018	1
Fe I	4961.92	3.63	-2.25	26.2	7.40	-	-	845	1	Fe I	6173.34	2.22	-2.88	67.7	7.57	56.9	7.18	62	1
Fe I	4962.58	4.18	-1.18	53.2	7.48	37.8	7.03	66	1	Fe I	6180.21	2.73	-2.65	53.3	7.50	-	-	269	1
Fe I	4973.10	3.96	-0.92	87.3	7.61	-	-	173	1	Fe I	6200.32	2.61	-2.44	72.2	7.58	-	-	207	1
Fe I	5022.24	3.98	-0.56	97.1	7.40	-	-	965	1	Fe I	6213.44	2.22	-2.48	81.0	7.45	-	-	62	1
Fe I	5029.62	3.41	-2.00	48.6	7.52	-	-	718	1	Fe I	6219.29	2.20	-2.43	89.5	7.55	-	-	62	1
Fe I	5044.22	2.84	-2.02	71.9	7.39	64.7	7.06	318	1	Fe I	6232.65	3.65	-1.22	81.0	7.58	73.6	7.29	816	1
Fe I	5074.75	4.22	-0.23	113.7	7.43	97.1	7.02	1094	1	Fe I	6240.65	2.22	-3.17	47.6	7.38	38.7	7.03	64	1
Fe I	5083.35	0.96	-2.96	109.7	7.40	-	-	16	1	Fe I	6246.33	3.59	-0.88	111.4	7.36	106.6	7.07	816	1
Fe I	5088.16	4.15	-1.75	37.0	7.63	-	-	1066	1	Fe I	6252.56	2.40	-1.69	119.2	7.40	106.8	7.00	169	1
Fe I	5141.75	2.42	-2.24	86.1	7.61	75.6	7.21	114	1	Fe I	6265.14	2.18	-2.55	84.0	7.54	76.5	7.22	62	1
Fe I	5145.10	2.20	-3.08	53.8	7.50	42.4	7.09	66	1	Fe I	6270.23	2.86	-2.61	51.0	7.52	42.0	7.19	342	1
Fe I	5198.72	2.22	-2.13	95.1	7.46	-	-	66	1	Fe I	6297.80	2.22	-2.74	74.4	7.56	65.5	7.22	62	1
Fe I	5217.40	3.21	-1.16	108.7	7.37	-	-	66	1	Fe I	6301.51	3.65	-0.72	113.9	7.57	106.4	7.27	816	1
Fe I	5225.53	0.11	-4.79	73.7	7.63	-	-	1	1	Fe I	6315.81	4.07	-1.66	40.3	7.51	24.6	7.03	1014	1
Fe I	5228.38	4.22	-1.26	syn	7.79	syn	7.18	1091	1	Fe I	6322.69	2.59	-2.43	75.3	7.60	64.3	7.22	207	1
Fe I	5242.50	3.63	-0.97	85.3	7.48	75.2	7.13	843	1	Fe I	6330.86	4.71	-0.97	33.2	7.23	21.1	6.85	1254	1
Fe I	5243.78	4.26	-1.12	61.1	7.59	49	7.22	1089	1	Fe I	6335.34	2.20	-2.18	97.0	7.42	85.9	7.03	62	1
Fe I	5247.06	0.09	-4.95	68.1	7.63	57.5	7.19	1	1	Fe I	6336.83	3.69	-0.86	102.2	7.32	93.9	6.99	816	1
Fe I	5250.22	0.12	-4.94	68.2	7.65	60.5	7.29	66	1	Fe I	6344.15	2.43	-2.92	50.2	7.38	-	-	169	1
Fe I	5250.65	2.20	-2.18	101.5	7.59	92.4	7.22	66	1	Fe I	6392.53	2.27	-4.03	17.1	7.51	-	-	109	3
Fe I	5253.47	3.28	-1.57	75.4	7.36	66.9	7.02	553	1	Fe I	6393.61	2.43	-1.58	130.4	7.42	-	-	168	1
Fe I	5288.53	3.69	-1.51	57.3	7.47	44.8	7.07	929	1	Fe I	6408.03	3.69	-1.02	syn	7.65	syn	7.23	816	1
Fe I	5298.78	3.64	-2.02	42.2	7.55	-	-	875	1	Fe I	6419.96	4.73	-0.27	80.5	7.41	70.2	7.10	1258	1
Fe I	5307.37	1.61	-2.99	86.0	7.58	76.2	7.19	36	1	Fe I	6430.86	2.18	-2.01	109.5	7.41	101.8	7.08	62	1
Fe I	5322.05	2.28	-2.80	60.3	7.44	-	-	112	1	Fe I	6469.19	4.83	-0.81	55.0	7.61	40.5	7.22	1258	1
Fe I	5365.41	3.57	-1.22	76.9	7.49	69.8	7.2	786	1	Fe I	6481.88	2.28	-2.98	63.7	7.59	55.0	7.26	109	1
Fe I	5373.71	4.47	-0.84	61.6	7.47	48.1	7.09	1166	1	Fe I	6498.94	0.96	-4.69	44.7	7.54	37.9	7.22	13	1
Fe I	5379.58	3.69	-1.51	60.8	7.54	44.3	7.04	928	1	Fe I	6518.37	2.83	-2.46	56.0	7.44	49.1	7.16	342	1
Fe I	5398.29	4.44	-0.71	72.5	7.51	59.4	7.13	553	1	Fe I	6593.88	2.43	-2.42	85.0	7.61	79.0	7.32	168	1
Fe I	5461.54	4.43	-1.88	26.0	7.74	-	-	1145	1	Fe I	6609.12	2.56	-2.69	64.2	7.57	54.9	7.23	206	1
Fe I	5473.91	4.15	-0.79	76.9	7.45	-	-	1062	1	Fe I	6678.00	2.69	-1.42	122.8	7.41	111.7	7.04	268	1
Fe I	5483.11	4.15	-1.41	46.5	7.47	-	-	1061	1	Fe I	6703.58	2.76	-3.06	36.6	7.52	26.9	7.16	268	1
Fe I	5487.15	4.41	-1.51	35.6	7.57	24.4	7.21	1143	1	Fe I	6750.16	2.42	-2.62	73.1	7.54	-	-	111	1

Table A2. Fe I and Fe II lines. The abundances were obtained for a model with $T_{\rm eff}$ = 5770 K, log g = 4.40 cgs, and ξ =0.66 km s^{-1} for the solar spectrum. $T_{\rm eff}$ = 5600 K, log g = 4.50 cgs, and ξ = 0.44 km s^{-1} for the HD 218209 spectrum.

Spec.	λ (Å)	LEP (eV)	log(gf) (dex)	Sun EW (mÅ)	Sun log ϵ(X) (dex)	HD 218209 EW (mÅ)	HD 218209 log ϵ(X) (dex)	RMT	Ref.
Fe I	6806.85	2.72	-3.21	34.0	7.57	25.2	7.22	268	1
Fe I	6810.28	4.59	-0.99	48.7	7.44	38.1	7.12	1197	1
Fe I	6820.43	4.62	-1.29	39.7	7.63	24.6	7.18	1197	2
Fe I	6862.48	4.54	-1.57	29.3	7.57	20.2	7.24	1191	3
Fe I	6898.31	4.20	-2.23	16.6	7.55	-	-	1078	3
Fe I	6916.70	4.14	-1.40	57.1	7.55	45.4	7.20	1052	1
Fe I	6977.44	4.57	-1.56	19.9	7.35	-	-	1225	3
Fe I	6999.90	4.09	-1.51	54.0	7.56	43.4	7.23	1051	2
Fe I	7016.07	2.41	-3.21	50.8	7.62	-	-	109	3
Fe I	7022.98	4.17	-1.20	63.5	7.48	50.6	7.11	1051	1
Fe I	7038.25	4.20	-1.25	60.0	7.49	-	-	1051	3
Fe I	7071.88	4.59	-1.70	26.5	7.67	18.6	7.37	1194	3
Fe I	7090.40	4.21	-1.16	64.5	7.49	50.0	7.10	1051	1
Fe I	7130.94	4.20	-0.80	87.3	7.46	73.0	7.08	1051	1
Fe I	7132.99	4.06	-1.63	41.6	7.47	31.3	7.13	1002	1
Fe I	7180.02	1.48	-4.78	20.0	7.52	-	-	1	3
Fe I	7212.47	4.93	-0.83	30.4	7.23	-	-	1273	3
Fe I	7219.69	4.07	-1.69	45.0	7.61	35.6	7.30	1001	3
Fe I	7221.22	4.54	-1.18	40.5	7.44	26.1	7.02	1189	3
Fe I	7222.88	4.59	-2.04	15.2	7.68	-	-	1187	3
Fe I	7228.70	2.75	-3.38	27.2	7.58	23.7	7.36	2	3
Fe I	7284.84	4.12	-1.57	41.6	7.46	27.8	7.04	1004	3
Fe I	7306.61	4.16	-1.44	42.0	7.37	30.3	7.00	1077	3
Fe I	7351.16	4.97	-0.84	36.2	7.40	23.0	7.00	1275	3
Fe I	7351.56	4.93	-0.64	45.5	7.36	34.3	7.04	1275	3
Fe I	7396.50	4.97	-1.64	12.6	7.53	-	-	1278	3
Fe I	7401.69	4.17	-1.35	40.9	7.26	-	-	1004	2
Fe I	7411.18	4.26	-0.30	101.9	7.43	-	-	4	3
Fe I	7418.67	4.12	-1.38	48.7	7.41	-	-	4	1
Fe I	7443.03	4.17	-1.82	34.7	7.59	28.0	7.33	1309	1
Fe I	7447.43	4.93	-0.85	34.1	7.32	24.8	7.02	1273	3
Fe I	7454.02	4.17	-2.41	12.0	7.51	-	-	5	3
Fe I	7473.56	4.59	-1.87	18.2	7.60	-	-	1188	3
Fe I	7491.68	4.28	-0.90	64.9	7.42	53.1	7.08	1077	3
Fe I	7498.56	4.12	-2.25	18.0	7.52	13.5	7.27	1001	3
Fe I	7511.05	4.16	0.09	151.6	7.46	141.1	7.14	1077	1
Fe I	7540.44	2.72	-3.85	11.5	7.51	-	-	266	3
Fe I	7551.10	5.06	-1.63	11.0	7.53	-	-	1303	3
Fe I	7568.93	4.26	-0.77	74.3	7.45	64.4	7.15	1077	3
Fe I	7583.80	3.00	-1.89	82.3	7.46	69.1	7.07	402	1
Fe I	7586.04	4.29	-0.47	112.3	7.74	106	7.48	1137	3
Fe I	7620.54	4.71	-0.66	55.4	7.38	-	-	1250	3
Fe I	7653.78	4.77	-0.89	34.4	7.21	-	-	1250	1
Fe I	7710.39	4.20	-1.11	64.9	7.54	61.0	7.36	1077	1
Fe I	7719.05	5.01	-1.15	28.3	7.55	19.2	7.23	1304	3
Fe I	7723.20	2.27	-3.62	42.2	7.65	-	-	108	2
Fe I	7745.48	5.06	-1.17	21.7	7.44	-	-	1305	3
Fe I	7748.28	2.94	-1.75	100.6	7.54	91.9	7.22	402	1
Fe I	7780.59	4.45	0.03	114.7	7.39	103.4	7.07	1154	3
Fe I	7832.22	4.42	0.11	118.0	7.31	112.0	7.06	1154	3
Fe I	7844.55	4.81	-1.70	12.8	7.43	-	-	1250	3
Fe I	7879.75	5.01	-1.47	10.2	7.27	-	-	1306	3
Fe I	7912.87	0.86	-4.84	48.3	7.56	36.0	7.12	12	1
Fe I	7941.09	3.26	-2.29	41.7	7.28	-	-	623	1
Fe I	7998.97	4.35	0.15	129.7	7.33	-	-	1136	3
Fe I	8028.34	4.45	-0.69	68.2	7.39	64.0	7.20	1154	3
Fe I	8047.60	0.86	-4.79	60.4	7.77	-	-	12	3
Fe I	8096.87	4.06	-1.78	35.1	7.41	-	-	999	1
Fe I	8204.10	0.91	-6.05	5.8	7.52	-	-	12	3
Fe I	8207.77	4.43	-0.86	65.4	7.48	47.4	7.02	1136	3
Fe I	8239.13	2.41	-3.18	44.9	7.38	36.4	7.07	108	3
Fe I	8248.15	4.35	-0.89	60.5	7.32	50.7	7.03	1136	3
Fe I	8293.53	3.30	-2.14	57.6	7.50	46.8	7.17	623	1
Fe I	8360.82	4.45	-1.29	57.2	7.74	45.3	7.41	1153	3
Fe I	8365.64	3.24	-1.91	69.0	7.45	55.4	7.06	623	1
Fe I	8424.14	4.93	-1.16	33.4	7.56	20.7	7.17	1272	3
Fe I	8439.60	4.53	-0.59	73.2	7.41	61.6	7.09	1172	3
Fe I	8514.08	2.19	-2.23	116.1	7.46	102.4	7.07	60	1
Fe I	8515.08	3.00	-2.07	83.0	7.64	71.4	7.30	401	2
Fe I	8526.68	4.89	-0.76	58.3	7.62	-	-	1270	1
Fe I	8582.27	2.98	-2.13	77.6	7.57	63.0	7.16	401	1
Fe I	8611.81	2.83	-1.85	98.5	7.41	83.9	7.02	339	1
Fe I	8613.93	4.97	-1.25	31.5	7.63	-	-	1272	3
Fe I	8616.27	4.89	-0.71	43.4	7.27	-	-	1266	3
Fe I	8699.43	4.93	-0.38	65.7	7.40	-	-	1267	1
Fe I	8757.19	2.83	-1.92	92.7	7.39	82.9	7.06	339	1
Fe I	8793.38	4.59	-0.09	107.9	7.45	98.3	7.16	1172	3
Fe I	8796.42	4.93	-1.23	27.3	7.46	-	-	1266	3
Fe I	8798.05	4.96	-1.89	8.0	7.47	-	-	1286	3
Fe I	8834.04	4.20	-2.59	8.0	7.44	-	-	1050	3
Fe I	8838.43	2.85	-1.87	97.5	7.42	83.9	7.04	339	1
Fe I	8846.82	4.99	-0.78	48.5	7.52	39.3	7.26	1267	3
Fe I	8878.26	2.98	-3.83	11.7	7.67	-	-	401	3
Fe I	8887.10	4.93	-1.94	4.8	7.25	-	-	1265	3
Fe I	8902.94	4.97	-2.11	8.6	7.73	-	-	1266	3
Fe I	8922.66	4.97	-1.70	12.9	7.53	-	-	1298	3
Fe I	8945.20	5.01	-0.22	72.2	7.40	49.6	6.91	1301	3
Fe I	8950.20	4.14	-2.43	13.1	7.46	-	-	1050	3
Fe I	8959.88	5.00	-1.84	8.9	7.50	-	-	1320	3
Fe I	8975.41	2.98	-2.22	77.3	7.60	-	-	400	1
Fe I	8984.87	5.08	-0.92	32.5	7.40	-	-	1301	3
Fe I	9010.55	2.60	-2.95	44.1	7.27	35.2	6.95	202	1
Fe I	9030.67	2.83	-3.64	25.5	7.77	-	-	338	1
Fe I	9070.42	4.20	-2.05	33.7	7.71	-	-	1076	3
Fe I	9079.60	4.63	-0.81	54.1	7.31	-	-	1172	3
Fe I	9089.41	2.94	-1.68	99.8	7.41	88.9	7.09	400	1
Fe I	9117.10	2.85	-3.46	32.3	7.76	-	-	338	3
Fe I	9156.23	3.00	-3.67	9.3	7.40	-	-	400	3
Fe I	9210.03	2.83	-2.40	65.0	7.37	-	-	83	2
Fe I	9382.93	4.96	-1.59	24.3	7.74	-	-	1284	3
Fe I	9602.07	4.99	-1.74	15.4	7.64	-	-	1283	3
Fe I	9653.14	4.71	-0.68	68.4	7.46	-	-	1247	3
Fe I	9753.13	4.77	-0.78	56.9	7.40	-	-	1247	3
Fe I	9786.62	4.59	-1.68	18.5	7.28	-	-	1171	3
Fe I	9800.34	5.06	-0.45	59.7	7.38	-	-	1292	3
Fe I	9861.79	5.04	-0.14	73.8	7.28	-	-	1296	1
Fe I	9881.51	4.56	-1.71	18.1	7.26	-	-	1209	3
Fe I	9889.08	5.01	-0.45	75.4	7.59	-	-	1296	1
Fe I	9944.13	4.99	-1.34	30.8	7.63	-	-	1285	3
Fe II	4178.86	2.58	-2.51	83.8	7.38	67.3	6.99	28	1
Fe II	4491.40	2.84	-2.64	74.8	7.50	-	-	37	1
Fe II	4508.29	2.85	-2.44	85.5	7.52	73.7	7.26	38	1
Fe II	4576.34	2.84	-2.92	63.8	7.48	-	-	38	1
Fe II	4582.83	2.84	-3.06	55.9	7.40	-	-	37	1
Fe II	4620.52	2.83	-3.19	52.0	7.41	37.1	7.03	38	1
Fe II	4993.36	2.79	-3.68	37.7	7.46	-	-	36	1
Fe II	5132.67	2.81	-4.09	25.1	7.53	14.6	7.20	35	1
Fe II	5197.58	3.23	-2.22	79.8	7.47	-	-	49	1
Fe II	5234.63	3.22	-2.21	82.1	7.49	67.7	7.19	49	1
Fe II	5264.81	3.33	-3.13	45.8	7.63	33.9	7.35	48	1
Fe II	5284.11	2.89	-3.11	syn	7.5	syn	6.98	41	1
Fe II	5325.56	3.21	-3.26	42.5	7.56	-	-	49	1
Fe II	5414.07	3.22	-3.58	28.2	7.49	15.7	7.12	48	1
Fe II	5425.26	3.20	-3.22	41.8	7.48	26.5	7.09	49	1
Fe II	5534.85	3.23	-2.75	57.4	7.46	39.3	7.02	55	1
Fe II	6084.11	3.19	-3.88	20.3	7.52	8.9	7.07	46	1
Fe II	6149.24	3.87	-2.84	35.9	7.57	23.2	7.25	74	1
Fe II	6238.38	3.87	-2.75	42.1	7.64	-	-	74	1
Fe II	6247.56	3.89	-2.30	52.0	7.46	38.2	7.16	74	1
Fe II	6432.68	2.89	-3.57	40.3	7.47	24.8	7.07	40	1
Fe II	6456.39	3.90	-2.05	62.1	7.45	46.6	7.12	74	1
Fe II	6516.08	2.89	-3.31	53.4	7.53	40.0	7.22	40	1
Fe II	7222.39	3.87	-3.40	18.9	7.60	-	-	73	1
Fe II	7224.51	3.87	-3.36	19.4	7.58	-	-	73	1
Fe II	7515.88	3.89	-3.39	13.1	7.38	-	-	73	1
Fe II	7533.42	3.89	-3.60	17.7	7.77	-	-	72	3
Fe II	7655.47	3.87	-3.77	7.1	7.41	-	-	73	3
Fe II	7711.71	3.89	-2.45	44.7	7.36	30.4	7.04	73	1

Table A3. The abundances were obtained for a model with $T_{\rm eff}$ = 5770 K, log g = 4.40 cgs, and ξ = 0.66 km s^{-1} for the solar spectrum. $T_{\rm eff}$ = 5600 K, log g = 4.50 cgs, and ξ = 0.44 km s^{-1} for the HD 218209 spectrum.

Spec.	λ (Å)	LEP (eV)	log(gf) (dex)	Sun EW (mÅ)	Sun log ϵ(X) (dex)	HD 218209 EW (mÅ)	HD 218209 log ϵ(X) (dex)	RMT	Ref.
C I	8335.19	7.65	-0.44	syn	8.41	syn	8.16	10	2
C I	9111.85	7.46	-0.34	syn	8.56	syn	8.34	3	4
O I	7771.96	9.11	0.37	syn	8.83	syn	8.73	1	2
O I	7774.18	9.11	0.22	syn	8.83	syn	8.74	1	2
O I	7775.40	9.11	0.00	syn	8.77	syn	8.69	1	2
Na I	5682.65	2.1	-0.7	syn	6.36	syn	5.87	6	2
Na I	5688.22	2.10	-0.37	122.1	6.11	101.1	5.73	6	4
Na I	6154.23	2.09	-1.55	36.9	6.27	22.9	5.89	5	2
Na I	8183.26	2.09	0.22	201.9	6.13	183.1	5.79	4	3
Mg I	4571.10	0.00	-5.40	syn	7.57	syn	7.58	1	5
Mg I	5711.10	4.34	-1.74	syn	7.63	syn	7.55	8	5
Mg I	7657.60	5.09	-1.27	syn	7.64	syn	7.45	22	2
Mg I	7691.57	5.73	-0.78	syn	7.65	syn	7.40	29	2
Mg I	8213.02	5.73	-0.51	syn	7.60	syn	7.47	28	2
Mg II	7896.37	9.96	0.64	syn	7.63	syn	–	8	2
Al I	6695.97	3.13	-1.57	syn	6.48	syn	6.17	5	2
Al I	6698.63	3.13	-1.87	syn	6.44	syn	6.07	5	2
Al I	7362.31	4.00	-0.79	syn	6.38	syn	6.17	11	6
Al I	7835.33	4.00	-0.69	syn	6.45	syn	6.19	10	6
Al I	7836.15	4.00	-0.50	syn	6.46	syn	6.19	10	6
Al I	8772.88	4.00	-0.35	syn	6.43	syn	6.28	9	6
Al I	8773.91	4.00	-0.16	syn	6.43	syn	6.28	9	6
Al I	8841.26	4.07	-1.50	syn	6.42	syn	6.16	15	2
Si I	5645.62	4.93	-2.03	35.0	7.49	25.1	7.23	10	7
Si I	5665.56	4.92	-1.99	39.7	7.53	28.6	7.25	10	7
Si I	5684.49	4.95	-1.58	60.1	7.51	46.3	7.21	11	7
Si I	5701.14	4.91	-2.05	38.5	7.55	28.8	7.31	10	2
Si I	5708.40	4.95	-1.47	72.1	7.59	60.1	7.33	10	2
Si I	5772.15	5.08	-1.62	51.1	7.51	40.7	7.27	17	7
Si I	5793.08	4.93	-1.86	43.2	7.47	30.1	7.16	9	7
Si I	5948.54	5.08	-1.09	83.0	7.49	70.9	7.23	16	7
Si I	6125.03	5.61	-1.53	30.6	7.50	23.1	7.30	30	7
Si I	6142.49	5.62	-1.48	33.6	7.51	23.8	7.27	30	7
Si I	6145.02	5.61	-1.39	37.0	7.48	27.8	7.26	29	7
Si I	6237.34	5.59	-0.98	58.7	7.41	46.1	7.16	28	3
Si I	6244.48	5.61	-1.29	44.3	7.51	30.9	7.23	28	7
Si I	6721.84	5.86	-0.94	42.2	7.32	–	–	–	2
Si I	7003.58	5.94	-0.59	58.1	7.48	46.8	7.27	60	2
Si I	7005.84	5.96	-0.59	72.8	7.48	67.4	7.35	60	2
Si I	7034.96	5.85	-0.88	63.8	7.59	51.0	7.35	50	3
Si I	7416.00	5.59	-0.75	87.1	7.45	–	–	22	3
Si I	7918.38	5.93	-0.61	79.7	7.58	–	–	57	6
Si I	9393.40	6.10	-1.53	13.3	7.35	–	–	72	3
Si I	9768.27	4.93	-2.68	27.0	7.78	–	–	7	3
P I	9525.78	6.98	-0.12	syn	5.56	syn	–	–	2
P I	9750.73	6.92	-0.20	syn	syn	–	–	2	2
P I	9796.79	6.99	0.19	syn	5.51	syn	–	–	2
S I	8693.98	7.84	-1.38	syn	7.15	–	–	6	2
S I	8694.70	7.84	0.05	syn	7.15	–	–	6	2
Ca I	4512.27	2.52	-1.90	23.6	6.29	–	–	24	3
Ca I	4526.94	2.70	-0.42	85.6	6.14	83.4	5.93	36	2
Ca I	4578.56	2.52	-0.70	82.8	6.27	–	–	23	8
Ca I	5260.39	2.52	-1.72	32.7	6.30	25.7	6.03	22	8
Ca I	5261.71	2.52	-0.58	98.6	6.47	90.7	6.18	22	8
Ca I	5512.99	2.93	-0.46	86.2	6.38	81.4	6.15	48	8
Ca I	5581.98	2.52	-0.56	92.9	6.34	–	–	21	8
Ca I	5590.13	2.52	-0.57	92.0	6.34	–	–	21	8
Ca I	6166.44	2.52	-1.14	70.3	6.33	68.2	6.13	20	8
Ca I	6169.04	2.52	-0.80	91.9	6.30	88.5	6.06	20	8
Ca I	6169.56	2.52	-0.48	108.7	6.19	109.5	5.97	20	8
Ca I	6439.07	2.51	0.39	160.0	6.07	157.1	5.80	18	2
Ca I	6455.60	2.52	-1.34	55.4	6.34	48.2	6.10	19	8
Ca I	6471.67	2.52	-0.69	90.5	6.36	88.2	6.17	18	8
Ca I	6493.79	2.52	-0.11	122.7	6.22	124.3	6.03	18	8
Ca I	6499.65	2.52	-0.82	86.1	6.41	80.8	6.18	18	8
Ca I	6572.79	0	-4.32	syn	6.32	syn	6.15	1	8
Ca I	7148.15	2.70	0.11	135.6	6.20	137.4	5.99	30	8
Ca I	7202.19	2.70	-0.26	108.2	6.26	–	–	29	3
Ca I	7326.15	2.92	-0.21	108.2	6.38	104.4	6.15	20	3
Ca I	9663.58	4.71	-0.69	6.5	6.22	–	–	55	3
Sc I	4023.69	0.02	0.38	syn	3.13	–	–	7	9
Sc II	4246.84	0.31	0.24	157.0	3.17	–	–	7	9
Sc II	5239.82	1.45	-0.76	syn	3.15	syn	2.82	26	9

Spec.	λ (Å)	LEP (eV)	log(gf) (dex)	Sun EW (mÅ)	Sun log ϵ(X) (dex)	HD 218209 EW (mÅ)	HD 218209 log ϵ(X) (dex)	RMT	Ref.
Sc II	5526.82	1.77	-0.01	75.3	3.32	68.0	3.13	18	9
Sc II	5640.99	1.5	-0.99	syn	3.12	syn	2.84	29	9
Sc II	5657.88	1.51	-0.54	67.1	3.39	57.4	3.14	29	9
Sc II	5667.15	1.50	-1.21	32.8	3.24	26.5	3.04	29	9
Sc II	5669.04	1.50	-1.10	34.2	3.16	28.1	2.97	29	9
Sc II	6245.63	1.50	-1.02	34.0	3.05	30.4	2.92	28	2
Sc II	6279.76	1.49	-1.33	28.6	3.22	21.0	2.97	28	3
Sc II	6300.70	1.50	-1.90	7.1	3.02	–	–	28	3
Sc II	6320.85	1.49	-1.82	9.0	3.05	–	–	28	3
Sc II	6604.60	1.35	-1.31	35.3	3.21	30.9	3.06	19	2
Ti I	4060.27	1.05	-0.69	syn	4.85	syn	4.51	80	10
Ti I	4186.13	1.5	-0.24	syn	4.89	syn	4.67	129	10
Ti I	4287.41	0.84	-0.37	68.6	5.02	73.2	4.94	44	10
Ti I	4453.32	1.43	-0.03	66.6	5.19	64.7	5.00	113	10
Ti I	4465.81	1.74	-0.13	39.2	4.89	33.9	4.62	146	10
Ti I	4512.74	0.84	-0.40	66.8	4.96	65.8	4.76	42	10
Ti I	4518.03	0.83	-0.25	73.5	4.96	74.6	4.80	42	10
Ti I	4534.79	0.84	0.35	96.4	4.84	100.8	4.65	42	10
Ti I	4548.77	0.83	-0.28	71.5	4.94	76.3	4.86	270	10
Ti I	4555.49	0.85	-0.40	64.1	4.89	66.3	4.78	266	10
Ti I	4617.28	1.75	0.44	62.6	4.89	60.5	4.70	145	10
Ti I	4623.1	1.74	0.16	syn	4.95	syn	4.58	145	10
Ti I	4639.36	1.74	-0.05	syn	4.94	syn	4.58	145	10
Ti I	4639.66	1.75	-0.14	syn	5	syn	4.59	145	10
Ti I	4656.47	0.00	-1.28	71.3	5.11	71.4	4.94	6	10
Ti I	4722.61	1.05	-1.47	19.3	5.03	–	–	75	10
Ti I	4742.80	2.24	0.21	31.2	4.82	31.4	4.70	233	10
Ti I	4758.12	2.25	0.51	42.9	4.81	45.1	4.74	233	10
Ti I	4759.28	2.25	0.59	46.3	4.81	44.9	4.65	233	10
Ti I	4820.41	1.50	-0.38	41.1	4.92	40.7	4.77	126	10
Ti I	4885.09	1.89	0.41	syn	4.93	syn	4.7	231	10
Ti I	4913.62	1.87	0.22	49.3	4.86	50.9	4.77	157	10
Ti I	4926.15	0.81	-2.17	6.6	4.92	–	–	39	2
Ti I	4981.74	0.85	0.57	112.8	4.81	–	–	38	10
Ti I	4999.51	0.83	0.32	103.4	4.90	–	–	38	10
Ti I	5009.65	0.02	-2.2	syn	4.87	syn	4.63	5	10
Ti I	5016.17	0.85	-0.48	64.7	4.92	67.2	4.81	38	10
Ti I	5020.03	0.83	-0.33	77.5	5.05	76.6	4.84	38	10
Ti I	5022.87	0.83	-0.33	71.3	4.90	72.4	4.75	38	10
Ti I	5039.96	0.02	-1.08	76.2	4.97	77.8	4.82	5	10
Ti I	5064.65	0.05	-0.94	85.3	5.08	80.9	4.78	294	10
Ti I	5145.47	1.46	-0.54	36.9	4.92	35.7	4.74	109	10
Ti I	5147.48	0.00	-1.94	37.1	4.87	38.5	4.71	4	10
Ti I	5152.19	0.02	-1.95	36.5	4.88	35.8	4.68	4	10
Ti I	5192.98	0.02	-0.95	83.9	5.00	–	–	4	10
Ti I	5210.39	0.05	-0.82	90.0	5.02	–	–	4	10
Ti I	5219.71	0.02	-2.22	28.1	4.95	–	–	4	10
Ti I	5490.16	1.46	-0.84	22.6	4.84	23.5	4.71	107	10
Ti I	5866.46	1.07	-0.79	47.9	4.98	–	–	72	10
Ti I	5918.55	1.06	-1.47	12.2	4.71	–	–	71	2
Ti I	5922.11	1.04	-1.47	20.1	4.96	22.6	4.86	72	2
Ti I	5978.54	1.87	-0.50	23.9	4.92	24.0	4.78	154	2
Ti I	6126.22	1.07	-1.42	21.6	4.97	24.4	4.88	69	10
Ti I	6258.11	1.44	-0.39	50.3	4.96	49.3	4.79	104	10
Ti I	6261.11	1.43	-0.53	46.5	5.01	46.1	4.85	104	10
Ti I	6336.11	1.44	-1.69	5.3	4.88	–	–	103	10
Ti I	6743.13	0.90	-1.63	18.4	4.88	–	–	32	10
Ti I	7216.20	1.44	-1.20	18.3	4.97	–	–	98	10
Ti I	7251.74	1.42	-0.76	33.7	4.89	31.7	4.69	99	10
Ti I	7357.74	1.44	-1.02	22.6	4.90	–	–	97	10
Ti I	8024.84	1.87	-1.08	10.6	4.94	–	–	151	10
Ti I	8364.24	0.83	-1.71	22.1	4.90	26.5	4.85	33	3
Ti I	8396.93	0.81	-1.63	25.2	4.88	27.0	4.76	33	3
Ti I	8412.36	0.81	-1.39	39.7	4.96	36.6	4.74	33	2
Ti I	8426.50	0.82	-1.20	53.0	5.03	54.7	4.91	33	2
Ti I	8434.98	0.84	-0.83	71.2	5.07	77.6	5.08	33	2
Ti I	8435.68	0.83	-1.02	61.7	5.06	66.0	5.02	33	2
Ti I	9027.32	1.73	-1.36	7.8	4.87	–	–	138	3
Ti I	9675.55	0.83	-0.80	78.6	5.04	70.7	4.76	32	3
Ti I	9718.96	1.50	-1.18	16.4	4.79	–	–	124	3
Ti I	9728.36	0.81	-1.21	47.2	4.82	–	–	32	3
Ti I	9770.28	0.84	-1.58	26.7	4.80	–	–	32	3
Ti I	9787.67	0.82	-1.44	40.3	4.92	–	–	32	3

Table A4. The abundances were obtained for a model with $T_{\rm eff}$ = 5770 K, $\log g$ = 4.40 cgs, and ξ = 0.66 km s^{-1} for the solar spectrum. $T_{\rm eff}$ = 5600 K, $\log g$ = 4.50 cgs, and ξ = 0.44 km s^{-1} for the HD 218209 spectrum.

Spec.	λ (Å)	LEP (eV)	$\log(gf)$ (dex)	Sun EW (mÅ)	Sun $\log\epsilon$(X) (dex)	HD 218209 EW (mÅ)	HD 218209 $\log\epsilon$(X) (dex)	RMT	Ref.	Spec.	λ (Å)	LEP (eV)	$\log(gf)$ (dex)	Sun EW (mÅ)	Sun $\log\epsilon$(X) (dex)	HD 218209 EW (mÅ)	HD 218209 $\log\epsilon$(X) (dex)	RMT	Ref.
Ti II	4443.81	1.08	-0.71	146.1	5.09	126.4	4.73	19	10	Ni I	4606.23	3.60	-1.02	syn	6.36	syn	5.89	100	2
Ti II	4468.50	1.13	-0.63	syn	5.21	syn	4.85	31	10	Ni I	4731.80	3.83	-0.85	42.7	6.28	31.3	5.92	163	2
Ti II	4493.53	1.08	-2.78	34.7	4.91	–	–	18	10	Ni I	4732.47	4.10	-0.55	42.2	6.24	–	–	235	2
Ti II	4568.33	1.22	-2.65	29.7	4.78	–	–	60	10	Ni I	4752.43	3.66	-0.69	syn	6.33	syn	5.8	132	2
Ti II	4583.41	1.16	-2.84	31.3	4.95	–	–	39	10	Ni I	4756.52	3.48	-0.34	syn	6.23	syn	5.74	98	2
Ti II	4708.67	1.24	-2.35	50.7	5.01	46.2	4.87	49	10	Ni I	4806.99	3.68	-0.64	59.4	6.30	47.9	5.93	163	2
Ti II	4874.01	3.09	-0.86	syn	4.95	syn	4.68	114	10	Ni I	4829.03	3.54	-0.33	77.1	6.17	67.4	5.83	131	2
Ti II	4911.20	3.12	-0.64	51.2	5.10	46.1	5.00	114	10	Ni I	4852.56	3.54	-1.07	syn	6.29	syn	5.92	130	2
Ti II	5005.17	1.57	-2.73	23.8	5.01	19.5	4.85	71	10	Ni I	4904.42	3.54	-0.17	84.9	6.14	74.7	5.79	129	2
Ti II	5336.79	1.58	-1.60	72.0	5.08	–	–	69	10	Ni I	4913.98	3.74	-0.62	53.9	6.20	41.5	5.82	132	2
Ti I	5418.77	1.58	-2.13	48.5	5.02	43.8	4.88	69	10	Ni I	4935.83	3.94	-0.36	58.5	6.20	48.9	5.89	177	2
V I	4437.84	0.29	-0.71	syn	3.89	syn	–	21	11	Ni I	4946.03	3.80	-1.29	25.9	6.29	15.2	5.87	148	2
V I	5727.06	1.08	-0.02	syn	3.89	–	–	35	11	Ni I	4953.21	3.74	-0.66	54.8	6.26	44.4	5.92	111	2
V I	6090.18	1.08	-0.07	syn	3.93	syn	3.52	34	2	Ni I	4998.23	3.61	-0.78	54.8	6.26	–	–	111	2
V I	6119.53	1.06	-0.36	syn	3.94	syn	3.6	34	11	Ni I	5010.94	3.63	-0.87	48.0	6.21	34.2	5.80	144	2
V I	6243.11	0.30	-0.94	syn	3.88	syn	3.52	19	11	Ni I	5032.73	3.90	-1.27	24.1	6.31	–	–	207	2
Cr I	4545.96	0.94	-1.38	83.5	5.70	75.5	5.33	10	2	Ni I	5035.37	3.63	0.29	97.6	5.91	89.5	5.60	143	2
Cr I	4616.13	0.98	-1.18	87.7	5.64	79.4	5.27	21	2	Ni I	5042.19	3.64	-0.57	59.0	6.15	51.0	5.85	131	2
Cr I	4626.18	0.97	-1.32	81.5	5.62	75.7	5.31	21	2	Ni I	5048.85	3.85	-0.37	syn	6.26	syn	5.86	195	2
Cr I	4646.17	1.03	-0.71	syn	5.71	syn	5.16	21	2	Ni I	5082.35	3.66	-0.54	63.6	6.23	–	–	130	2
Cr I	4651.29	0.98	-1.46	78.3	5.69	72.9	5.40	21	2	Ni I	5084.10	3.68	0.03	89.1	6.10	–	–	162	2
Cr I	4652.17	1.00	-1.03	99.7	5.72	90.5	5.34	21	2	Ni I	5088.54	3.85	-0.91	32.1	6.12	–	–	190	2
Cr I	4708.02	3.17	0.11	58.0	5.58	44.0	5.16	186	2	Ni I	5102.97	1.68	-2.62	47.3	6.12	–	–	49	2
Cr I	4718.42	3.19	0.10	65.8	5.75	55.0	5.40	186	2	Ni I	5115.40	3.83	-0.11	74.8	6.17	60.6	5.76	177	2
Cr I	4730.72	3.08	-0.19	48.5	5.65	37.1	5.28	145	2	Ni I	5155.13	3.90	-0.66	49.0	6.27	35.2	5.86	206	2
Cr I	4737.35	3.07	-0.10	55.5	5.65	42.7	5.25	145	2	Ni I	5435.87	1.99	-2.60	50.9	6.47	40.7	6.10	70	2
Cr I	4756.12	3.10	0.09	63.2	5.76	54.2	5.44	145	2	Ni I	5587.87	1.93	-2.14	syn	6.23	syn	5.69	70	2
Cr I	4936.34	3.11	-0.34	44.8	5.73	31.8	5.31	166	2	Ni I	5593.75	3.90	-0.84	42.0	6.27	–	–	206	2
Cr I	4964.93	0.94	-2.53	38.6	5.65	27.3	5.21	9	2	Ni I	5625.33	4.09	-0.70	39.0	6.25	24.5	5.82	221	2
Cr I	5247.57	0.96	-1.63	83.4	5.79	72.6	5.38	18	2	Ni I	5637.12	4.09	-0.80	33.8	6.23	21.4	5.83	218	2
Cr I	5296.70	0.98	-1.41	93.5	5.77	79.7	5.31	18	2	Ni I	5641.89	4.10	-1.08	23.5	6.27	–	–	234	2
Cr I	5300.75	0.98	-2.13	58.4	5.72	45.4	5.26	18	2	Ni I	5682.21	4.10	-0.47	51.5	6.29	37.7	5.90	232	2
Cr I	5345.81	1.00	-0.98	114.5	5.68	–	–	18	2	Ni I	5748.36	1.68	-3.26	29.1	6.26	–	–	45	2
Cr I	5348.33	1.00	-1.29	99.8	5.77	–	–	18	2	Ni I	5805.23	4.17	-0.64	40.4	6.29	24.6	5.83	234	2
Cr I	5787.93	3.32	-0.08	45.2	5.60	31.8	5.19	188	2	Ni I	6007.32	1.68	-3.34	24.9	6.21	17.6	5.85	42	2
Cr I	6925.24	3.43	-0.33	37.9	5.75	–	–	222	2	Ni I	6086.29	4.26	-0.51	42.3	6.27	29.4	5.89	249	2
Cr I	6926.04	3.43	-0.62	20.5	5.61	–	–	222	3	Ni I	6108.12	1.68	-2.44	65.2	6.27	55.1	5.91	45	2
Cr I	6979.82	3.45	-0.41	34.7	5.74	–	–	222	2	Ni I	6128.98	1.68	-3.32	25.3	6.20	17.0	5.81	42	2
Cr I	7400.23	2.89	-0.11	75.4	5.58	–	–	93	2	Ni I	6130.14	4.26	-0.96	21.1	6.22	14.6	5.93	248	2
Cr I	8348.28	2.70	-1.87	13.1	5.83	–	–	56	3	Ni I	6175.37	4.09	-0.54	47.4	6.24	33.7	5.85	217	2
Cr I	8947.20	3.09	-0.75	28.1	5.49	–	–	142	3	Ni I	6176.82	4.09	-0.53	63.1	6.53	–	–	228	2
Cr I	8976.88	3.07	-1.03	18.5	5.50	–	–	142	3	Ni I	6204.61	4.09	-1.14	20.9	6.23	–	–	226	2
Cr I	9290.44	2.53	-0.88	58.6	5.69	–	–	29	3	Ni I	6322.17	4.15	-1.17	17.4	6.20	10.3	5.84	249	2
Cr I	9730.32	3.54	-0.77	12.9	5.45	–	–	226	3	Ni I	6327.60	1.68	-3.15	41.5	6.40	27.2	5.92	44	2
Cr I	9900.87	2.97	-2.14	5.2	5.81	–	–	80	3	Ni I	6378.26	4.15	-0.90	31.7	6.31	–	–	247	2
Cr II	4588.20	4.07	-0.65	70.9	5.67	–	–	44	12	Ni I	6414.59	4.15	-1.21	17.2	6.24	–	–	244	2
Cr II	4616.64	4.05	-1.29	45.2	5.65	31.7	5.33	44	2	Ni I	6482.81	1.93	-2.63	41.1	6.11	27.9	5.67	66	2
Cr II	5237.32	4.07	-1.17	53.2	5.76	35.3	5.33	43	12	Ni I	6598.61	4.23	-0.98	24.3	6.28	15.2	5.92	249	2
Cr II	5305.87	3.83	-1.91	25.2	5.50	14.4	5.17	24	12	Ni I	6635.14	4.42	-0.83	24.6	6.32	17.6	6.04	264	2
Mn I	4055.55	2.14	-0.08	syn	5.47	syn	4.92	5	13	Ni I	6767.78	1.83	-2.17	77.9	6.41	–	–	57	2
Mn I	4082.94	2.18	-0.36	syn	5.55	syn	4.84	5	13	Ni I	6772.32	3.66	-0.99	48.5	6.26	–	–	127	4
Mn I	4451.59	2.89	0.28	syn	5.47	syn	4.83	22	13	Ni I	6914.56	1.94	-2.27	77.9	6.56	–	–	62	2
Mn I	4470.14	2.94	-0.44	syn	5.49	syn	4.92	22	13	Ni I	7030.06	3.53	-1.83	19.8	6.33	–	–	126	3
Mn I	4502.22	2.92	-0.34	syn	5.34	syn	4.74	22	13	Ni I	7110.91	1.93	-2.97	36.2	6.30	24.5	5.88	64	2
Mn I	4709.72	2.89	-0.49	syn	5.36	syn	4.75	21	13	Ni I	7385.24	2.73	-1.96	45.2	6.28	33.5	5.91	84	2
Mn I	4739.11	2.94	-0.61	syn	5.39	syn	4.73	21	13	Ni I	7422.30	3.62	-0.13	90.5	5.99	–	–	139	2
Mn I	4765.86	2.94	-0.09	syn	5.45	syn	4.75	21	13	Ni I	7522.78	3.64	-0.47	73.9	6.29	66.6	6.04	126	3
Mn I	4766.42	2.92	0.10	syn	5.41	syn	4.83	21	13	Ni I	7525.14	3.62	-0.43	69.0	6.14	57.7	5.81	139	3
Mn I	4783.42	2.30	0.03	syn	5.60	syn	4.84	16	13	Ni I	7555.60	3.83	0.05	90.3	6.23	77.6	5.88	187	3
Mn I	5117.94	3.13	-1.20	syn	5.45	–	–	32	13	Ni I	7574.08	3.82	-0.45	63.5	6.23	49.5	5.84	156	3
Mn I	5432.55	0.00	-3.79		5.33	syn	4.73	1	13	Ni I	7727.66	3.66	-0.17	87.2	6.23	70.5	5.82	156	3
Mn I	6013.50	3.06	-0.25	syn	5.46	syn	4.8	27	2	Ni I	7748.93	3.69	-0.18	84.5	6.22	75.8	5.94	156	3
Mn I	6021.80	3.07	-0.05	syn	5.56	syn	4.94	27	13	Ni I	7797.62	3.88	-0.18	75.1	6.22	63.8	5.90	201	3
Co I	4121.33	0.92	-0.33	syn	5.05	–	–	28	14	Ni I	8965.94	4.09	-0.89	39.4	6.30	–	–	225	3
Co I	4792.86	3.24	0.00	syn	4.89	syn	4.54	158	3	Cu I	5105.54	1.38	-1.50	syn	4.25	syn	3.8	2	2
Co I	4813.48	3.21	0.12	syn	5.04	syn	4.59	158	14	Cu I	5218.20	3.80	0.26	syn	4.11	syn	3.56	3.57	2
Co I	5352.05	3.58	0.06	syn	4.89	syn	4.40	172	14	Cu I	7933.13	3.77	-0.37	syn	4.21	–	–	6	3
Co I	5483.36	1.71	-1.50	syn	4.94	syn	4.54	39	14	Cu I	8092.63	3.80	-0.04	syn	4.23	syn	3.72	6	3
Co I	5647.23	2.27	-1.56	syn	4.94	syn	4.46	112	2	Zn I	4722.16	4.03	-0.39	syn	4.64	syn	4.49	2	15
Co I	6093.15	1.74	-2.40	syn	4.94	–	–	37	14	Zn I	4810.54	4.08	-0.17	syn	4.63	syn	4.42	2	15
Co I	8093.93	4.00	0.29	syn	4.94	syn	4.38	189	2	Sr I	4607.34	0.00	0.28	syn	2.84	syn	2.29	2	16
Ni I	4410.52	3.31	-1.08	55.6	6.33	–	–	88	2	Y II	4883.69	1.08	0.07	syn	2.3	syn	1.8	22	17
Ni I	4470.48	3.40	-0.40	80.5	6.24	71.5	5.90	86	2	Y II	5087.43	1.08	-0.17	syn	2.27	syn	1.74	20	17

Table A5. The abundances were obtained for a model with $T_{\rm eff}$ = 5770 K, log g = 4.40 cgs, and ξ = 0.66 km s^{-1} for the solar spectrum. $T_{\rm eff}$ = 5600 K, log g = 4.50 cgs, and ξ = 0.44 km s^{-1} for the HD 218209 spectrum.

Spec.	λ (Å)	LEP (eV)	log(gf) (dex)	Sun EW (mÅ)	Sun log ϵ(X) (dex)	HD 218209 EW (mÅ)	HD 218209 log ϵ(X) (dex)	RMT	Ref.	Spec.	λ (Å)	LEP (eV)	log(gf) (dex)	Sun EW (mÅ)	Sun log ϵ(X) (dex)	HD 218209 EW (mÅ)	HD 218209 log ϵ(X) (dex)	RMT	Ref.
Zr I	4772.32	0.62	0.04	syn	2.53	–	–	43	3	Ce II	4042.14	0.50	0.00	syn	1.60	–	–	252	2
Zr II	4208.98	0.71	-0.46	syn	2.6	–	–	41	18	Ce II	4562.37	0.48	0.21	syn	1.63	syn	1.49	1	20
Zr II	4050.32	0.71	-1.06	syn	2.62	syn	2.29	43	3	Ce II	4628.16	0.52	0.14	syn	1.56	–	–	1	20
Ba II	4554.04	0.00	0.14	syn	2.3	syn	1.99	1	19	Nd II	4021.33	0.32	-0.10	syn	1.38	–	–	36	3
Ba II	5853.69	0.60	-0.91	syn	2.33	syn	1.98	2	19	Nd II	4446.40	0.20	-0.35	syn	1.33	syn	1.07	49	3
La II	4086.72	0.00	-0.07	syn	1.2	syn	0.76	10	2	Nd II	4567.61	0.20	-1.31	syn	1.37	–	–	49	3
La II	4662.51	0.00	-1.25	syn	1.13	–	–	8	2	Sm II	4519.63	0.54	-0.35	syn	0.94	syn	0.72	49	21
La II	4748.73	0.92	-0.54	syn	1.1	syn	0.83	65	2	Sm II	4577.69	0.25	-0.65	syn	0.96	–	–	23	21

References for the adopted gf-values: (1) Fuhr & Wiese (2006), (2) NIST Atomic Spectra Database (http://physics.nist.gov/PhysRefData/ASD), (3) VALD, (4) Takeda et al. (2003), (5) Pehlivan Rhodin et al. (2017), (6)Kelleher & Podobedova (2008), (7) Shi et al. (2011), (8) Den Hartog et al. (2021), (9) Lawler et al. (2019), (10) Lawler et al. (2013), (11) Lawler et al. (2017), (12) Lawler et al. (2017), (13) Den Hartog et al. (2011), (14) Lawler et al. (2015), (15) Biemont & Godefroid (1980), (16) Hansen et al. (2013), (17) Hannaford et al. (1982), (18) Biemont et al. (1981), (19) Klose et al. (2002), (20) Lawler et al. (2009), (21) Lawler et al. (2006)

Table A6. Solar abundances from the literature. The abundances for species in bold type face are obtained via spectrum synthesis.

Species	log $\epsilon_{\odot}$(X†) (dex)	n	log $\epsilon_{\odot}$(X*)	n	ASP09/ASP21 (1),(2)	LOD (3)	GRE (4)	CAF (5-10)	HOL (11)	BIE (12)	LAM (13)
C I	**8.50±0.07**	**2**	-	-	8.43±0.05 / 8.46±0.04	8.39±0.04	8.39±0.05	8.50±0.06	8.592±0.108	8.60±0.10	8.67±0.10
O I	**8.85±0.04**	**3**	-	-	8.69±0.05 / 8.69±0.04	8.73±0.07	8.66±0.05	8.76±0.07	8.736±0.078	-	8.92±0.04
Na I	6.17±0.09	3	6.16±0.07	2	6.24±0.04 / 6.22±0.03	6.30±0.03	6.17±0.04	-	-	-	-
Mg I	**7.64±0.06**	**5**	7.60±0.08	2	7.60±0.04 / 7.55±0.03	7.54±0.06	7.53±0.09	-	7.538±0.060	-	-
Mg II	**7.67±0.00**	**1**	-	-	7.60±0.04/ 7.55±0.03	7.54±0.06	7.53±0.09	-	-	-	-
Al I	**6.45±0.02**	**8**	-	-	6.45±0.03 / 6.43±0.03	6.47±0.07	6.37±0.06	-	-	-	-
Si I	7.50 ±0.09	21	7.50±0.07	12	7.51±0.03 / 7.51±0.03	7.52±0.06	7.51±0.04	-	7.536±0.049	-	-
P I	**5.44±0.00**	**1**	-	-	5.41±0.03 / 5.41±0.03	5.46±0.04	5.36±0.04	5.46±0.04	-	-	-
S I	**7.15±0.00**	**2**	-	-	7.12±0.03 / 7.12±0.03	7.14±0.01	7.14±0.05	7.16±0.05	-	-	-
Ca I	6.29±0.10	20	6.34±0.08	18	6.34±0.04 / 6.30±0.03	6.33±0.07	6.31±0.04	-	-	-	-
Sc I	3.13±0.00	1	3.12±0.00	1	3.15±0.04 / 3.14±0.04	3.10±0.10	3.17±0.10	-	-	-	-
Sc II	3.18±0.11	10	3.23±0.08	7	3.15±0.04 / 3.14±0.04	3.10±0.10	3.17±0.10	-	-	-	-
Ti I	4.92±0.09	56	4.96±0.09	43	4.95±0.05 / 4.97±0.05	4.90±0.06	4.90±0.06	-	-	-	-
Ti II	4.99±0.10	9	4.99±0.08	12	4.95±0.05 / 4.97±0.05	4.90±0.06	4.90±0.0	-	-	-	-
V I	**3.92±0.02**	**5**	3.99±0.05	5	3.93± 0.08 / 3.90±0.08	4.00±0.02	4.00±0.02	-	-	-	-
Cr I	5.67±0.10	28	5.71±0.07	19	5.64±0.04 / 5.62±0.04	5.64±0.01	5.64±0.10	-	-	-	-
Cr II	5.64±0.11	4	5.64±0.14	3	5.64±0.04 / 5.62±0.04	5.64±0.01	5.64±0.10	-	-	-	-
Mn I	5.61±0.16	11	5.62±0.13	13	5.43±0.05 / 5.42±0.06	5.37±0.05	5.39±0.03	-	-	-	-
Fe I	7.49±0.11	252	7.54±0.09	132	7.50±0.04 / 7.46±0.04	7.45±0.08	7.45±0.05	7.52±0.12	7.448±0.082	7.54±0.03	7.48±0.09
Fe II	7.49±0.09	28	7.51±0.04	17	7.50±0.04 / 7.46±0.04	7.45±0.08	7.45±0.05	7.52±0.06	-	7.51±0.01	-
Co I	**4.96±0.06**	**8**	-	-	4.99±0.07 / 4.94±0.05	4.92±0.08	4.99±0.07	-	-	4.92±0.08	4.92±0.08
Ni I	6.24±0.10	60	6 .28±0.09	54	6.22±0.04 / 6.20±0.04	6.23±0.04	6.23±0.04	-	-	-	-
Cu I	**4.19±0.06**	**4**	-	-	4.19±0.02 / 4.18±0.05	4.21±0.04	4.21±0.04	-	-	-	-
Zn I	**4.63±0.00**	**2**	4.68±0.03	2	4.56±0.05 / 4.56±0.05	4.62±0.15	4.60±0.03	-	-	4.60±0.03	4.60±0.08
Sr I	**2.89±0.00**	**1**	2.91±0.00	1	2.87±0.07 / 2.83±0.06	2.92±0.05	2.92±0.05	-	-	-	-
Y II	**2.28±0.01**	**2**	2.29±0.05	2	2.21±0.05 / 2.21±0.05	2.21±0.02	2.21±0.02	-	-	-	-
Zr II	**2.59±0.08**	**2**	2.68±0.00	1	2.58±0.04 / 2.59±0.04	2.58±0.02	2.58±0.02	-	-	2.56±0.05	-
Ba II	**2.29±0.06**	**2**	2.24±0.06	4	2.18±0.09 / 2.27±0.05	2.17±0.07	2.17±0.07	-	-	-	-
La II	**1.11±0.06**	**3**	-	-	1.10±0.04 / 1.11±0.04	1.14±0.03	1.13±0.05	-	-	-	-
Ce II	**1.59±0.04**	**3**	1.64±0.02	2	1.58±0.04 / 1.58±0.04	1.61±0.06	1.70±0.10	-	-	1.70±0.04	-
Nd II	**1.37±0.01**	**3**	1.42±0.05	3	1.42±0.04 / 1.42±0.04	1.45±0.05	1.45±0.05	-	-	-	-
Sm II	**0.96±0.02**	**2**	0.96±0.00	1	0.96±0.04 / 0.95±0.04	1.00±0.05	1.00±0.03	-	-	-	-

X†: This study (TS), X*: Şahin et al. (2023), (1) Asplund et al. (2009), (2) Asplund et al. (2021), (3) Lodders et al. (2009), (4) Grevesse et al. (2007), (5) Caffau et al. (2007), (6) Caffau et al. (2008), (7) Caffau et al. (2009), (8) Caffau et al. (2010), (9) Caffau et al. (2011), (10) Caffau et al. (2019), (11) Holweger (2001), (12) Biemont et al. (1993), (13) Lambert (1978).

Table A7. The elemental abundances of HD 218209 from the literature for respective elements.

Species	TS24 (1)	TA23 (2)	RI20 (3)	LU17 (4)	DA15 (5)	MI11/13 (6)	TA07 (7)	VA05 (8)	MI04 (9)	GE04 (10) (LTE/NLTE)	AB88 (11)
C I	0.14	-0.08	0.18		-0.01						
O I	0.28	0.08	0.42			0.22					
Na I	-0.03		0.03	0.06		-0.02		0.10		0.23/0.16	
Mg I	0.24		0.17	0.29	0.18	0.19			0.19	0.41/0.43	
Al I	0.13		0.21	0.26		0.26				0.27/0.47	0.45
Si I	0.13		0.17	0.15	0.15	0.18	0.26	0.20	0.18		0.18
Ca I	0.15		0.12	0.19	0.13	-0.35					0.26
Sc II	0.06			0.15							
Ti I	0.21		0.24	0.21	0.20		0.03	0.23			
V I	-0.02		0.17	0.16	0.13		0.03				
Cr I	-0.02		-0.07	0.03							
Cr II	0.01										
Mn I	-0.27		-0.27	-0.14	-0.16						
Co I	-0.10			0.08			0.13				
Ni I	-0.02		0.01	-0.01		0.04	0.00	0.01	0.04		0.19
Cu I	-0.13			-0.03	-0.07	-0.02					
Zn I	0.20			0.12		0.14					
Sr I	-0.18			0.10							
Y II	-0.14		0.02	0.08		-0.04					
Zr II	0.05			0.26		0.01					
Ba II	0.04			0.04		-0.01					
La II	0.03			0.63		0.09					
Ce II	0.26			0.28		-0.02					
Nd I	0.08			0.32		0.15					
Sm II	0.14			0.26		0.13					

(1) This Study, (2) Takeda (2023, TA23), (3) Rice & Brewer (2020, RI20), (4) Luck (2017, LU17), (5) da Silva et al. (2015, DA15), (6) Mishenina et al. (2011, MI11), (6) Mishenina et al. (2013, MI13), (7) Takeda et al. (2007, TA07), (8) Valenti & Fischer (2005, VA05), (9) Mishenina et al. (2004, MI04), (10) Gehren et al. (2004, GE04), (11) Abia et al. (1988, AB88).

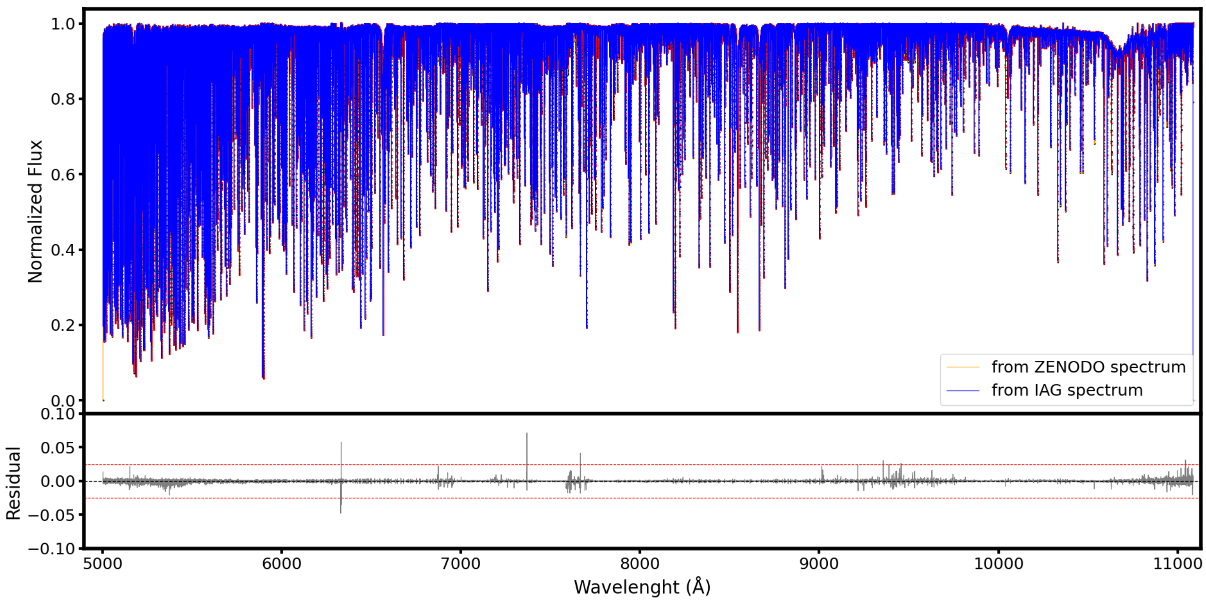

Figure A1. The normalized blue colour spectrum is the IAG spectrum, and the red colour spectrum is the ZENODO spectrum.

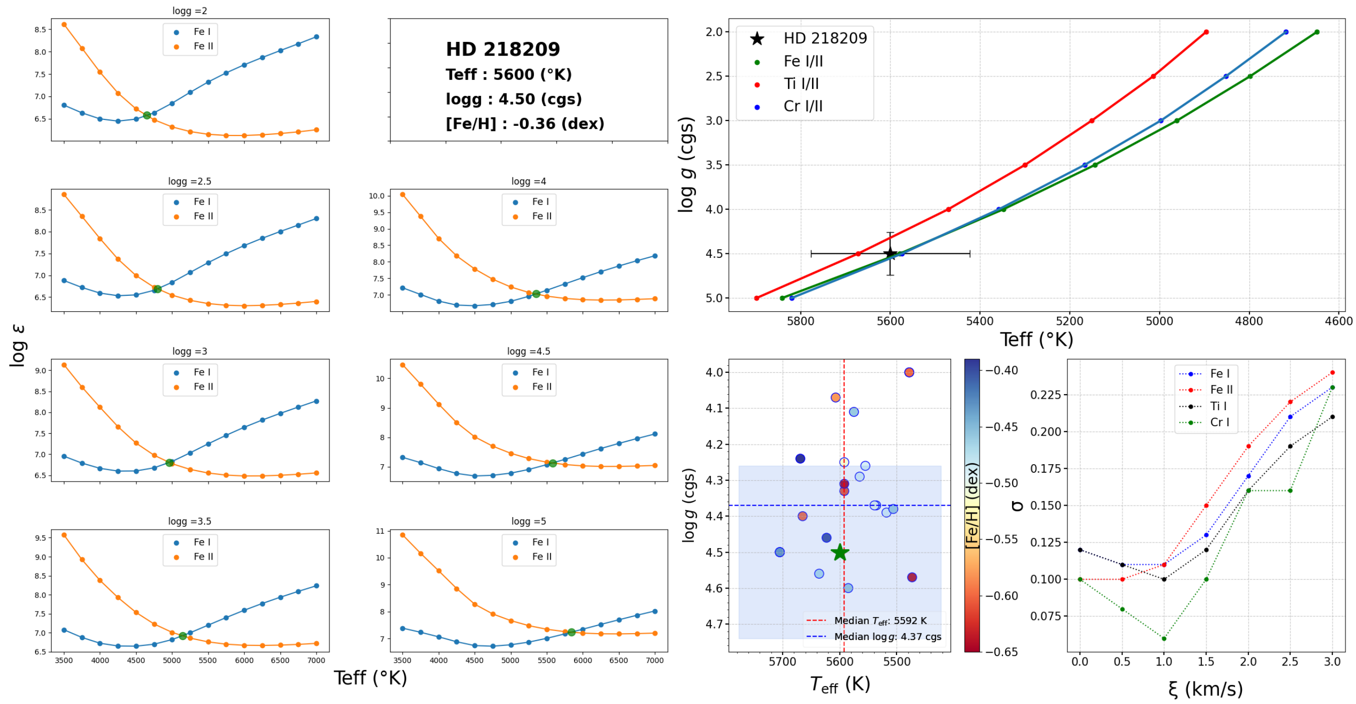

Figure A2. The dispersion test for Ti, Cr, and Fe. The standard deviations of Ti, Cr, and Fe abundances for a suite of the Ti I, Cr I, Fe I, and Fe II lines as a function of ξ were provided. The stellar parameters reported in the literature for the star exhibit large variations (the middle panel). The faint blue area in the image represents errors in the model parameters.